THESIS FOR THE DEGREE OF LICENTIATE OF ENGINEERING

Green aromatics for a bio-based economy

Valorization of biomass derived model compounds over zeolites studied by online analysis

Christopher Sauer

CHALMERS

Department of Chemistry and Chemical Engineering
CHALMERS UNIVERSITY OF TECHNOLOGY
Gothenburg, Sweden 2021

Green aromatics for a bio-based economy

Valorization of biomass derived model compounds over zeolites studied by online analysis

Christopher Sauer

Licentiatuppsatser vid Institutionen för kemi och kemiteknik

Chalmers tekniska högskola

Nr 2021:03

Department of Chemistry and Chemical Engineering
Chalmers University of Technology
SE-412 96 Gothenburg
Telephone +46 31 772 1000

Typeset in LaTeX using the kaobook class
Printed by Chalmers Reproservice
Gothenburg, Sweden 2021

Green aromatics for a bio-based economy
Valorization of biomass derived model compounds over zeolites studied by online analysis

Christopher Sauer
Department of Chemistry and Chemical Engineering
Chalmers University of Technology

Abstract

In the strive towards a sustainable chemical production, its carbon-based products can no longer be produced from fossil resources but need to be manufactured from a renewable feedstock. Simple aromatic building blocks like benzene, toluene and xylenes (BTX) can be obtained by catalytic valorization of biomass derived platform molecules such as furans provided efficient catalysts can be formulated.

To evaluate catalysts for the conversion of furans to BTX and study the involved catalytic reactions, advanced analytical methods are needed. The observation of dynamic responses in catalytic activity and selectivity necessitates time-resolved analysis of rather complex hydrocarbon (HC) streams.

In this work, an online analysis method combining Fourier transform infrared spectroscopy and ion molecule reaction mass spectrometry has been developed for the direct monitoring of the effluent stream during conversion of furans over zeolite catalysts. The sampling frequency is shown to be at least $4\,\mathrm{min}^{-1}$, which is considerably higher compared to that of separation-based methods operating on time scales of several minutes. A wide range of HCs and other smaller molecules is identified and individual species quantified simultaneously. The carbon balance of around 90% shows that the vast majority of the complex HC stream is indeed analysed.

The developed online analysis has been applied to catalytic step-response experiments, where different zeolites were exposed to concentration steps of 2,5-dimethylfuran at steady temperatures. It is found that the HC stream consists of a range of olefins and aromatics, including BTX. Most interestingly, 2,5-dimethylfuran is isomerized to 2,4-dimethylfuran as well as 2- and 3-methyl-2-cyclopenten-1-one. The formation of BTX is linked to the availability of olefins, which is supported by temperature programmed desorption experiments.

Furthermore, to build understanding of the catalytic mechanisms, surface species were characterised *in situ* by use of diffuse reflectance infrared Fourier transform spectroscopy. It is clear that upon adsorption, 2,5-dimethylfuran interacts with the zeolite structure and undergoes transforming reactions to olefins and aromatics upon temperature increase, but further studies are necessary to comprehend how the rather low selectivity towards BTX can be increased by catalyst design.

Keywords: biomass conversion, online analysis, zeolite, 2,5-dimethylfuran, catalysis

List of Manuscripts

This thesis is based on the following appended papers:

I. On-line composition analysis of complex hydrocarbon streams by time-resolved Fourier transform infrared spectroscopy and ion-molecule reaction mass spectrometry

Christopher Sauer, Anders Lorén, Andreas Schaefer and Per-Anders Carlsson

In manuscript

II. Valorization of 2,5-dimethylfuran over zeolites studied by on-line FTIR-MS analysis

Christopher Sauer, Anders Lorén, Andreas Schaefer and Per-Anders Carlsson

In manuscript

My Contributions to the Manuscripts

Paper I

I was responsible for planning and performing all experimental work and data analysis, except of the GC–MS analysis. I interpreted the results together with my co-authors and wrote the first draft of the manuscript.

Paper II

I was responsible for planning and performing all experimental work and data analysis. I interpreted the results together with my co-authors and wrote the first draft of the manuscript.

Contents

Notation

δ(X)	Symmetric in-plane bending, scissoring, of group X
ν_s(X)	Symmetric stretching of group X
ν_{as}(X)	Asymmetric stretching of group X
BAS	Brønsted acid site
BTX	Benzene, Toluene, Xylenes
CFP	Catalytic fast pyrolysis
DACD	Diels Alder cycloaddition dehydration
dmf	Dimethylfuran
DRIFTS	Diffuse reflectance infrared Fourier transform spectroscopy
EI	Electron ionization
FTIR	Fourier transform infrared
GC	Gas chromatography
HC	Hydrocarbon
IMR	Ion molecule reaction
LAS	Lewis acid site
m/z	Mass to charge ratio
MFC	Mass flow controller
MS	Mass spectrometry
SAR	SiO_2 to Al_2O_3 ratio
TOS	Time on stream
TPD	Temperature programmed desorption

List of Figures

List of Tables

1 Introduction

The rapidly growing global population [1], warming of the earth, climate change [2] and loss of biodiversity [3] caused by human activities are existential threats to our ecosystems and human societies.

Rapid action is needed to develop our economies and societies in more sustainable ways. This is evident on a political level for example by the United Nations Framework Convention on Climate Change or the "European Green Deal", where the EU strives for climate neutrality by 2050. [4] How can this change be accelerated? One answer is catalysis.

In a colloquial speech, a catalyst is known as something that causes, facilitates or accelerates change.[1] Such a catalyst might be necessary to facilitate the change in our societies and industries. The scientific definition states that a catalyst accelerates a chemical reaction. This happens by forming bonds with the reacting molecules. The reacting molecules form a product, which detaches from the catalyst. In this overall process, the catalyst remains unaltered, being available for catalysing the next cycle. [6]

1: Urban dictionary: "somebody or something that makes a change happen or brings about an event". [5]

Simplified, in an uncatalyzed reaction, a reaction proceeds when reactants collide with sufficient energy to overcome the energy barrier E_a as shown in the blue curve in figure 1.1. The difference in potential energy between reactants and products is the change in enthalpy (ΔH). The heterogeneous catalytic reaction, on the other hand, starts by adsorption of the reactant(s) on the catalyst surface on the so-called active site. The formation of the product follows, again with overcoming an activation barrier which is, however, significantly lower than that of a uncatalyzed reaction. In a final endothermic step, the product(s) separates from the catalyst. An alternative pathway is thus offered by introducing several elementary steps, that is more complex compared to the uncatalyzed reaction, but energetically favourable. The overall change in free energy is however the same. This means, that the catalyst accelerates the reaction rate kinetically, but does not change the equilibrium of a reaction, *i.e.* the thermodynamics.

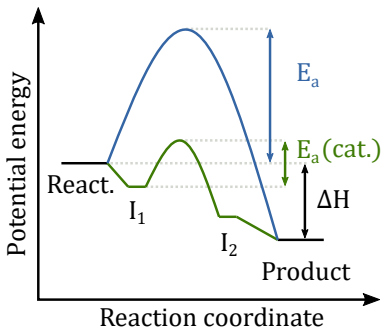

Figure 1.1: Schematic energy diagram for a catalyzed and non catalyzed reaction, where E_a is the activiation energy, ΔH the enthalpy and I an intermediate.

Today catalysis is involved in the production of any bulk chemical. Almost all carbon-based materials are derived from oil and its fossil friends. Catalysis is involved in the efficient transformation of all these compounds. Indeed, until now has the biggest part of catalysis contributed to the rapid growth of the global population[2] and the use of fossil resources. The transition to a sustainable

2: Through the invention of the Haber-Bosch process to produce ammonia from nitrogen and hydrogen to make fertilizers. [7]

economy needs to look at all aspects where fossil resources are used. In the chemical industry, the production of the majority of bulk chemicals is based on crude oil. During refining processes, the crude oil is transformed into industrial products mostly as energy sources, such as jet fuel, petrol and diesel but also building blocks for the chemical industry. A big fraction of these building blocks are so-called BTX aromatics, benzene, toluene and xylenes which make up about 15%. [8]

But catalysts do also help reduce energy consumption and the formation of undesired waste products by increasing efficiency and selectivity. Catalysis is a powerful tool to make this rapid change happen to help mitigate climate change. [9] For this transition, sustainable carbon sources are available, such as waste and biomass forest products and can play one part in the whole transition.[3] The use of the latter can be overall positive when harvested responsibly and the protection of local ecosystems is taken into consideration.

3: Replacement of fossil resources can complement the 5 R:
Refuse
Reduce
Reuse
Repurpose
Recycle

1.1 Motivation of this work

When shifting from fossil-based feedstocks for chemical production towards renewable resources, new chemical pathways have to be explored and made industrially viable. Renewable feedstocks such as wooden biomass exist and even offer forest-rich countries like Sweden independence from importing oil and oil-based products for the manufacture of chemicals. Value can be created not only monetary by upgrading biomass to chemical building blocks but also by shifting from fossil exploitation to a circular bio-based economy. This motivates research aiming at the question of how catalysis can be applied for the efficient conversion of biomass. To explore one such approach the reader is invited to Chapter 2, where the background and objective of this thesis are explained.

Background 2

This chapter covers the scope of this work and will briefly introduce the conceptual ingredients on which this thesis is based. Biomass-derived chemicals, zeolite materials as catalysts and the so produced aromatic hydrocarbons are the classes of materials described here. The catalytic process will be described and its analysis discussed.

2.1 Biomass-derived feedstocks

Plant biomass consists primarily of cellulose, hemicellulose and lignin. [10] Cellulose is a crystalline linear polysaccharide of glucose monomers, while hemicellulose is an amorphous polysaccharide built mainly from xylose. Lignin, however, is a large polyaromatic polymer. Because of their polymerous nature and their high oxygen content, these materials require significant upgrades before the aromatic building blocks suitable for our technology can be obtained. Furans, a class of 5-membered cyclic carbohydrates, can be derived from the cellulosic feedstock. These furanic compounds have been identified as model platform molecules from which many other compounds can be derived and incorporated into the existing production processes. [11]

2,5-dimethylfuran (2,5-dmf) is one of these model compounds. One pathway to obtain the platform molecule is presented in figure 2.1. The route starts with the depolymerization and hydrolysis of (hemi)cellulose to release the monomeric building blocks, such as the monosaccharide glucose. Subsequent isomerization of glucose to fructose is achieved using enzyme or heterogeneous catalysis. [1] The conversion of fructose to 5-hydroxymethylfurfural follows. [14] Finally, hydrodeoxygenation gives 2,5-dimethylfuran with high selectivity of 98%. [15] Other furans like furan and 2-methylfuran can be obtained in similar ways. [12, 16]

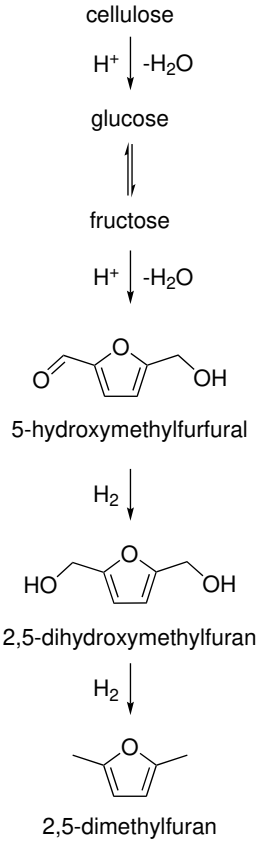

Figure 2.1: Established pathway to 2,5-dimethylfuran. [12]

2.2 Zeolites

Zeolites are microporous, crystalline aluminosilicates with a three-dimensional framework structure. The first reference of these materials is from the Swedish mineralogist Axel Fredrik Cronstedt, who coined the term *zeolite* in 1756. [17] TO_4-tetrahedrons[2] are the primary units of the zeolite structure. These units are organized to

1: A heterogeneous base or Lewis acid catalyst such as the zeolite Sn-BEA. [13]

Zeolite, from Greek $\zeta\epsilon\omega$ (zeo), meaning "to boil" and $\lambda\iota\theta o\varsigma$ (lithos), meaning "stone" due to their ability to store big amounts of water and releasing it as steam when heated. [17]

2: Where T are Si or Al atoms.

3: A three-letter code assigned by the International Zeolite Association to label different structure types. [18]

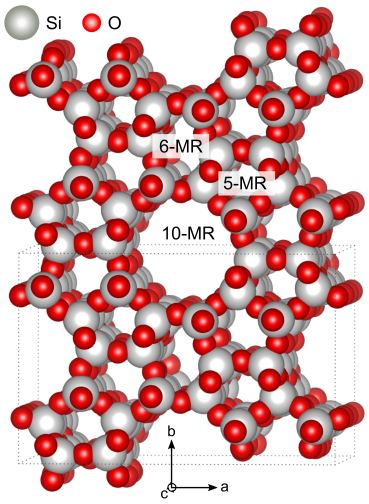

Figure 2.2: Visualization of the MFI type framework structure showing different channels.

Table 2.1: Some characteristics of chosen zeolites.[19]

zeolite	code	ring	size [Å]
Y	FAU	12	7.4
ZSM-5	MFI	10	5.1
		10	5.3
beta	BEA	12	6.6
		12	5.6

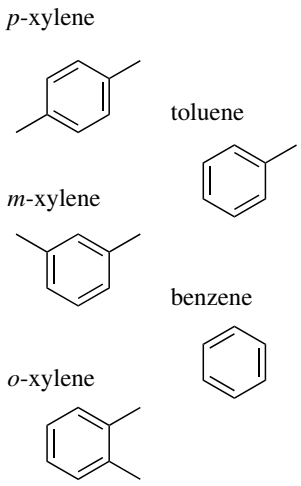

Figure 2.3: Representation of BTX aromatics.

form channels, cages and cavities. There are many different ways in how the structures are composed and today more than 200 types of framework structures are known. [18] The micropores can be of different dimensions depending on the number of tetrahedrons involved. For example, some of the zeolites used in this work show the MFI[3] framework structure, which is characterized by 10, 6, 5 and 4-membered rings (MR) as shown in figure 2.2.

Depending on the size and shape of the ring, the resulting various pore sizes make various zeolites versatile in different applications. Some zeolites and their characteristics are shown in table 2.1.

In the above-mentioned tetrahedron a net negative charge is induced, when T is an Al atom. This negative charge must be balanced by a counter ion. These counter ions can be changed in a process called ion-exchange, for example replacing a Na^+ ion with a proton or a Cu-ion. Protons as counter ions give acidic property to zeolites, which is why they are known as solid acids. The species Si−O(H)−Al is known as a Brønsted acid site (BAS). As follows, by increasing the Al-content in the framework, the amount of BAS increases.

Lewis acid sites (LAS) can be generated by using metals as counter ions such as Na^+ or Ga^{3+}. Also, dehydration, the loss of an Al-bound hydroxy group, for example after increased temperature, creates a LAS.

Beside these versatile characteristics when it comes to acidity, zeolites are selective to molecules of certain sizes due to the shape and size of their channels and cages. [20] Zeolites exhibit further high thermal stability . [19, 20] The latter applies especially to silica-rich zeolites, which makes them suitable for catalysis at high temperatures. They can frequently be regenerated under oxidative treatment and are non-corrosive and not toxic. [19]

As solid acid catalysts, zeolites play a major role in many catalytic processes, [21] and have been a material of choice for the traditional production of aromatics in petroleum refining due to their tunable acidity and shape selectivity, which is based on their unique structures. [22] Their first application in petroleum industry is the use of montmorillonite as a catalyst in the Houdry cracking process in 1936 years after their acidic nature was discovered by R. Kobayashi in 1902. [8]

2.3 Aromatic BTX

Benzene, Toluene and Xylenes aromatics are to date to the largest extent produced from fossil fuels via petroleum refining and

catalytic reforming. [23] They are among the most produced bulk chemicals in the world with a global market value of $186 billion in 2018 and growing. [24, 25] The production in Europe alone corresponds to more than 12 million tons per year. [26] BTX are, beside their unprocessed use as solvents and fuel additives, among the most important building blocks for many important fine chemicals and polymers, such as polystyrene, nylon, polyurethane and polyethene terephthalate. [27]

2.4 Catalytic process

Diels-Alder Cycloaddition Dehydration

In the future, we cannot rely on fossil resources as feedstocks for aromatic production any longer. When finding new routes to synthesize these products we need to follow the principles of green chemistry. Instead of breaking down complex molecules and rebuild them from C_1 or C_2 fragments, chemical complexity should be preserved. This can be achieved, as shown in figure 2.4, through a Diels-Alder[4] reaction, a thermally allowed [4+2]-cycloaddition (DAC) to form a bicyclic intermediate called oxa-norbornene, followed by a dehydration reaction (D), in the following referred to as the Diels-Alder cycloaddition dehydration (DACD). This preserves the complexity of the already existing 5-membered ring and upgrades it to a 6-membered ring with a perfect carbon efficiency and only water as a byproduct.

The applied Diels-Alder reaction to furans and alkenes was found to be catalyzed by Lewis acid sites (LAS) but not by Brønsted acid sites (BAS).[29] However, the dehydration reaction of the oxa-norbornene is so slow that it does not occur at reasonable rates. It can be catalyzed by Lewis-Acids and tremendously by Brønsted acids as shown in figure 2.5. Summarizing the current literature, it can be stated that the route to *p*-xylene is kinetically limited by cycloaddition when using BAS and by dehydration when using LAS.[29–31] The conditions in high-pressure batch reactors containing a mixture of a zeolite catalyst, 2,5-dimethylfuran, gaseous ethene and a solvent such as n-heptane, have been continuously proven to be highly selective towards *p*-xylene.[32] Yields up to 90% using zeolite beta,[33] or 93% using tin phosphate have been reported.[34]

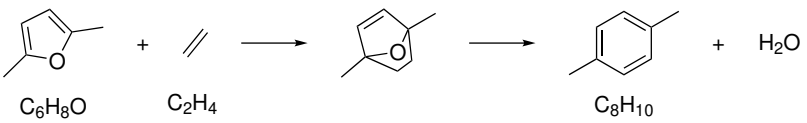

Figure 2.4: Diels Alder Cycloaddition Dehydration reaction.[28, 29]

4: First described by Otto Diels and Kurt Alder in 1928 and later honoured with the Nobel Prize in Chemistry 1950.

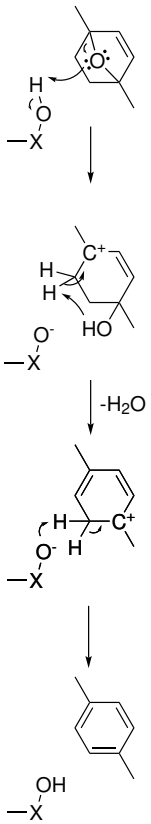

Figure 2.5: Acid catalyzed dehydration.[28, 29]

Catalytic Fast Pyrolysis

Another way to produce aromatics from biomass directly or furans as model compounds is the catalytic fast pyrolysis (CFP). In this approach the feedstock is rapidly heated, vaporized and then directed to a catalyst bed of zeolites where it reacts at high temperatures.

In CFP biomass or furanic model compound is fed into a fluidized bed reactor and heated rapidly where it thermally decomposes to form vapours. These vapours enter a zeolite catalyst in the same fluidized bed reactor to be converted to aromatic compounds, olefins, CO along with CO_2, water and coke.[35, 36]

The aromatization process under these conditions is complex. Many different cracking, oligomerization, isomerization, decarbonylation and dehydration reactions are taking place.[37] Even though the aromatic formation has been observed with moderate yields, the involvement of DACD is debated.[38, 39] Further in-depth studies are required to shine light on the mechanisms of the many reactions involved and how the selectivity towards desired products can be increased while rapid catalyst deactivation can be avoided.

To date, the industrial application of aromatics production from furanic biomass is scarce compared to that from the traditional refining industry. However, the first industrial (test) plants are in use.[40, 41]

2.5 On-line analysis

The two main approaches (DACD and CFP) described above are dominating the current literature on the formation of aromatics from furans. Both methods rely on *ex situ* analysis of the reaction products by gas chromatography-mass spectrometry (GC-MS) for identification and by GC flame ionization detection (FID) and/or thermal conductivity detection (TCD) for quantification. The DACD approach in high pressured batch reactors requires collection of a liquid sample via a double block sampling system from the proceeding reaction and pretreatment before analysis.[30, 33] In CFP studies, heavy products are collected using an air bath condenser and gas-phase products are collected in airbags. Condensed heavy products and gas-phase products are then identified by GC-MS and quantified by GC-FID/TCD.[37, 42–45] The sampling frequencies of these methods are usually around several minutes. In response, an approach was presented by Uslamin *et al.* where the reactor outlet is connected to an on-line GC-FID/TCD analyzer in tandem with a MS.[38, 39, 46, 47] Despite the on-line approach, the time-resolution is at best still limited to several minutes, which is a

general characteristic of separation-based methods, although they are often superior when it comes to stand-alone identification.

When studying catalytic reactions, it is of particular interest to investigate the transient response of dynamic processes, *e.g.*, composition variations in process streams upon changes in catalyst activity, selectivity and fast deactivation phenomena. For the observation of these phenomena fast analysis methods are needed. The direct and on-line analysis of the product stream upon changes in various process parameters can indicate mechanistic pathways. All in all, facilitating our understanding of how the catalyst material and its structure influence activity and selectivity. This is of special importance as the manifold of reaction mechanisms in the CFP are not yet fully understood. Only when the behaviour of model compounds is understood, the real biomass streams can be optimized based on rational catalyst design. The on-line analysis will be of interest even for industrial application as a tool for process analytical technology to monitor processes in a production plant.

2.6 Objective of the thesis

The objective of this thesis is to develop a method that allows for on-line analysis of complex hydrocarbon (HC) streams, obtained from the catalytic conversion of the biomass model compound 2,5-dimethylfuran. Fourier transform infrared spectroscopy (FTIR) and mass spectrometry are chosen techniques thanks to the possibility of high time resolution. The method shall then be applied to analyze real catalytic experiments on aromatics production from furans. The knowledge from this analysis is expected to help to understand the complex reaction mechanisms when probing zeolite catalyst with organic molecules. Other *in situ* analytical techniques, *e.g.* surface-sensitive tools, are used as investigation methods to complement and widen the understanding of such reactions and catalyst deactivation processes. These are necessities to make rational decisions about future catalyst design for biomass conversion.

Methodology 3

In this work, the product stream of furanic conversion is studied by on-line analysis. Two analytical techniques, infrared spectroscopy and mass spectrometry are applied for speciation and quantification of the gas composition. This chapter briefly introduces the theoretical basis and the analytical techniques. Further, the used catalyst materials, the reactor setup and calibration procedures are described.

3.1 Infrared spectroscopy

Infrared (IR) spectroscopy is based on the interaction of infrared light with matter. The measurement of absorption, transmission T or reflectance R of the incident light is used to identify chemical substances or their functional groups, and is applied to solids, liquids and gases. Absorption occurs when the frequency of the light source matches the frequency of the molecular vibration, so-called resonant frequency. The vibrations in chemical bonds can be described as an anharmonic oscillator and have several vibrational modes.[1] The six normal vibration modes of the CH_2-part of a CH_2R_2 molecule are shown in table 3.1. The frequencies are further affected by the shape of the molecule and the mass of the atoms involved in the chemical bond. An IR active vibrational mode must include a change in the dipole moment.[2] By examining the transmitted or reflected light the sample's absorption can be obtained. The transmission (reflectance) is defined as the fraction of intensity of the incident light I_0 and the transmitted (reflected) light I as described in equation (3.1). Absorption is usually expressed as absorbance (A), the logarithm of reciprocal transmission (or reflectance) as denoted in equation (3.2)

The magnitude of the absorbance is approximated by the Beer-Lambert law in equation (3.3), where ϵ is the molecule specific extinction coefficient, l the sample thickness and c the sample concentration. From this equation, a linear relationship between the absorbance and the concentration is evident. This is a reliable approximation, although some exceptions exist when the law can breakdown, such as at very high analyte concentrations. [48] For the on-line analysis of the complex HC stream, a gas phase FTIR spectrometer (MKS MultiGas 2030) was used.

1: The number of vibrational modes for a molecule with N number of atoms is 3N – 5 for linear and 3N – 6 for non-linear molecules.

2: Example: N_2 is not IR active while H_2O has 3 degrees of vibrational modes.

$$T = \frac{I}{I_0} \tag{3.1}$$

$$A = \log_{10} \frac{1}{T} \tag{3.2}$$

$$A = \epsilon l c \tag{3.3}$$

Table 3.1: Presentation of the 6 normal modes of vibrations for the CH_2-part of a CH_2R_2 molecule.

Symmetric	Antisymmetric
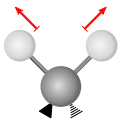 Stretching ν_s	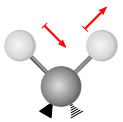 Stretching ν_{as}
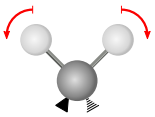 Scissoring δ	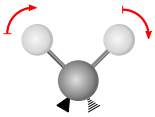 Rocking ρ
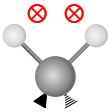 Wagging ω	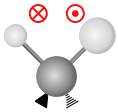 Twisting τ

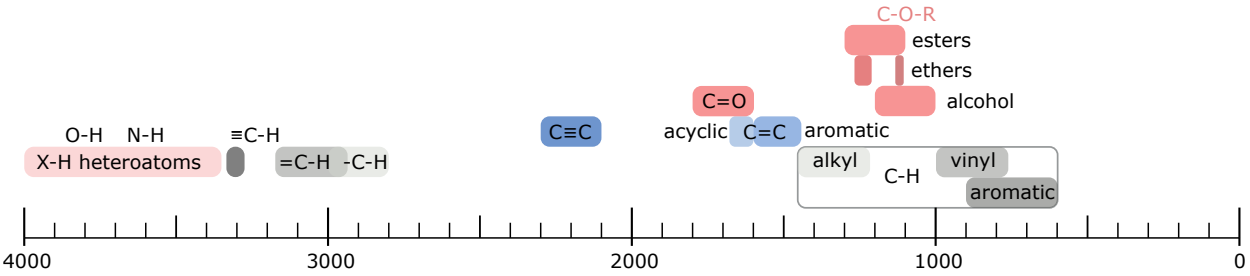

Figure 3.1: Characteristic infrared frequencies of functional groups in organic molecules containing C, O, N, X and H atoms

Group frequencies

As described before, molecules have vibrational modes. These are characteristic of common types of chemical bonds and functional groups. The group's frequency or absorption band is typically reported in wavenumbers (cm^{-1}) and is dependent on the bond strength and the mass of the atoms involved in the chemical bond. Figure 3.1 summarizes a few typical group frequencies observed in the experiments of this work.[49] The scope is limited to organic molecules consisting of H, C and O-atoms, but the illustration still shows the complexity of IR-spectroscopy. The analysis of a mixture of many different molecules is thus challenging and requires tedious selection and comparison of the absorption bands.

A commercial FTIR spectrometer is aimed to be used for the analysis of complex hydrocarbon streams, which includes a commercial reference compound library. Many organic and inorganic species are part of this library in forms of their IR spectra and corresponding concentrations. For this type of hydrocarbon stream, several species of interest are, however, not included in the library. These missing compounds are systemically calibrated and added to the reference compound library. The primary analysis band of each compound has to be chosen carefully so that no overlap of compounds with similar absorbance bands should occur.

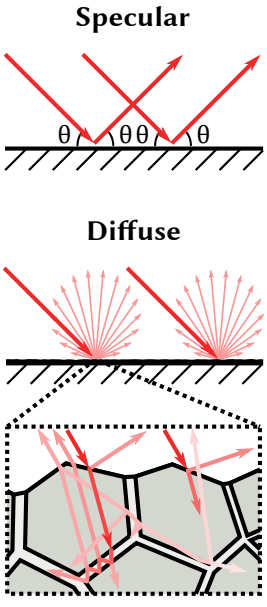

Figure 3.2: Schematic illustration for the difference between specular and diffuse reflection. The "zoom" is an example of some internal reflections of a polycrystalline material. Reproduced with permission from Felix Hemmingsson.

Diffuse Reflectance

Besides specular reflection, where the incident lights' angle equals the reflections angle, there is diffuse reflection (figure 3.2). This type of reflection is produced by the samples rough surface's reflection in all directions and is observed for finely ordered materials such as powders. The distribution of rays is collected by parabolic mirrors. Because of the diffuse reflection of a powder's many surfaces, molecular surface species can be studied, which makes this technique suitable for *in situ* experiments. This technique is also referred to as diffuse reflectance infrared Fourier transform spectroscopy (DRIFTS). For *in situ* infrared experiments a Bruker

Vertex 70 FTIR spectrometer was used in diffuse reflectance mode to reveal surface species.

3.2 Mass spectrometry

Mass spectrometry is an analytical tool widely applied for the identification and monitoring of pure samples and complex mixtures. In principle, the sample is vaporized, if not already in gas form. Subsequently, the sample gas is ionised to form charged particles. This can be done by different techniques. Electron ionization (EI), which is categorized as a hard ionization technique, applies an electron beam, which interacts with the sample to produce ions. The comparably high energy of the electron beam can break chemical bonds, resulting in a high degree of fragmentation of the sample molecules. This means that apart from the parent ion[3] the molecule breaks apart into many different fragments or so-called daughter ions. In the analyzer of the spectrometer, a magnetic field directs the produced ions through a filter to separate them by their mass-to-charge ratio (m/z). The selection of sorted ions is passed to the detector, which is the final stage of a mass spectrometer. Here, the ions induce charge or produce current and thereby the abundance of each ion is recorded. With this information at hand, the chemical composition of the sample can be determined, for example by comparing the resulting mass spectra to databases. On one hand, a high fragmentation pattern is useful for single molecular samples because the fragmentation pattern is specific for each molecule. On the other hand, many fragments are undesirable when analyzing a mixture of molecules when a separation is not possible prior to MS. This could be the case when doing on-line monitoring of production processes or catalytic studies.

3: which is the intact sample molecule, just in its ionic form

Some examples of mass selection are sector field, time-of-flight, quadrupole mass analyzers and ion traps.

Ion-molecule reaction mass spectrometry

When less fragmentation is desired, other ionization techniques, usually referred to as soft ionization, is required. Ion molecule reaction mass spectrometry (IMR-MS) is one such soft ionization method. In a separate chamber, an atomic gas is ionized to form a primary ion via EI, which is then directed to the sample stream. Here, the primary gas ion (G^+) reacts with the sample molecule (A) to produce a sample ion A^+ via a charge transfer ion-molecule reaction (equation (3.4)). [50]

$$G^+ + A \rightarrow G + A^+ \qquad (3.4)$$

Since the gas ions have much lower energy compared to EI, fewer bonds in the sample molecule will break and the fragmentation pattern is less complex. Further, because the ionization potential of the sample molecule must be lower than the ion energy of

Table 3.2: Ion potentials of different gases used in IMR-MS compared to electron ionization EI.

Ionizer	ion. potential /eV
EI	70
Kr	14.00
Xe	12.13
Hg	10.44

Example: Krypton ions (14.0 eV) can separate N_2 (15.6 eV) against CO (13.7 eV) on mass 28. [51]

the gas ion, different sample molecules can be selectively ionized with different gas ions, such as Hg, Xe or Kr. Based on the theory, efforts have been made to develop gas analyzers, that are suitable for simultaneous detection of many complex species. [50, 51] A similar instrument has been used for the on-line analysis of the complex HC stream and for desorption experiments (V&F Airsense Compact) .

3.3 Gas Chromatography

4: Usually an inert or non-reactive gas such as He or N_2.

Gas chromatography (GC) is a technique for the separation and subsequent analysis of compounds, that can be vaporized. A so-called *mobile phase*[4] carries the analyte through a stationary phase, a glass or metal tubing with microscopic layers of liquid or polymer fastened on a solid support. The principle of GC is based on the interaction of analytes with the stationary phase depending on their physical and chemical properties. This interaction is different for the various types of analytes letting the compounds exit the column at different times leading to a desired separation. This is known as the retention times, which is used to analyze a mixture by GC. Gas chromatographs might further be equipped with a detector, of which the most common ones are the flame ionization detector (FID) and the thermal conductivity detector (TCD) both being sensitive to a wide range of compounds. One of the most powerful combinations is the coupling of GC for separation and MS for analysis, known as GC–MS. Even for the smallest amounts of sample, this technique is highly effective and sensitive.

3.4 Catalyst preparation

Table 3.3: Catalyst characteristics.

catalyst	SiO_2/Al_2O_3
H-BEA	38
H-ZSM-5	330
H-ZSM-5	55
Cu-ZSM-5*	27
**2 wt% Cu.* [52]	

Four different zeolite materials have been studied as catalysts in this work as shown in table 3.3. This selection represents two different pore size channels by having a representative of the MFI and BEA type of framework structure, as well as different acidities according to their SiO_2/Al_2O_3 ratios (SAR). ZSM-5 of the MFI type and zeolite beta of the BEA type have been continuously used to study the conversion of furans to aromatics due to their shape selectivity favouring the BTX yields. [33, 42] To study the effect of a metal counterion, Cu has been introduced into the H-ZSM-5 sample by ion-exchange. [52] The studied materials are summarized in table 3.3 The catalyst in powder form was wash-coated onto a monolithic ceramic substrate (Cordierite, 400 cpsi, 7 mil, Corning) with a length of 1.5 cm and a diameter of approximately 1.2 cm. This process started with preparing a slurry of catalyst, binder and water. The monolith substrate was dipped into this slurry and

calcined in sequence several times until the desired amount of catalyst was deposited on the monolith surface.

One of the design principles of a catalyst is that it should have a high surface area accessible to the reactants. By coating the monolithic ceramic substrate with an even and thin catalyst layer, diffusion effects, concentration gradients and pressure drops can be minimized by exposing as much of its surface to the gas phase as possible.

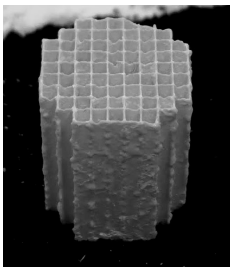

Figure 3.3: A catalyst sample coated on a monolith substrate.

3.5 Reactor setup

A continuous flow reactor was used for some of the experiments in this thesis and is schematically displayed in figure 3.4. The reactor setup consists of various inlet gases, whose flow rates are controlled with mass flow controllers (MFC). Argon is used as a balance gas to allow for an inert environment free of oxygen and water. The inlet feed of the liquid reactant such as 2,5-dimethylfuran is controlled with a gasifier setup: argon gas, whose flow rate is controlled with an MFC, streams through a gasifier that is filled with the liquid reactant. The gasifier is made of glassware and has an inner volume of 4 mL. The carrier gas and the liquid reactant mix forming saturated vaporized gas according to the liquid reactant's vapour pressure. The mixture, which is assumed to be in equilibrium is continuously transported into the reactor cell.

The vapor pressure p, given in mmHg of a compound is calculated for any temperature[5] with the Antoine equation (3.5), where T is the temperature in °C and the coefficients A, B and C are compound specific parameters (see table 3.4).

5: In the range of 16.78 °C to 283.98 °C for 2,5-dmf

$$\log_{10} p = A - \frac{B}{C + T} \tag{3.5}$$

Table 3.4: Antoine coefficients for 2,5-dmf. [53]

A	= 7.057412399
B	= 1265.510066
C	= 210.0001503

After the gasifier setup, all tubing is insulated and equipped with heating bands to avoid condensation. Between the gasifier and the reactor cell sits an electronic controllable switch, which can direct the reactant stream either to the reactor cell or the exhaust. This enables stabilisation of the reactant concentration and by-passing the reactor prior to dosing to the reactor, which allows a constant and stable flow of the reactant.

The reactor cell consists of a quartz glass tube surrounded by a heating coil. The monolithic substrate coated with the catalyst is placed within. One thermocouple is inserted in front of the monolith to control the reactor temperature. A second thermocouple is inserted near the catalyst surface to observe the catalyst temperature. After passing the reactor cell, the gas stream is directed to an ion-molecule reaction mass spectrometer (Airsense Compact, V&F) and a gas phase FTIR analyzer (MKS MultiGas 2030), which are used in parallel to analyze the gas stream.

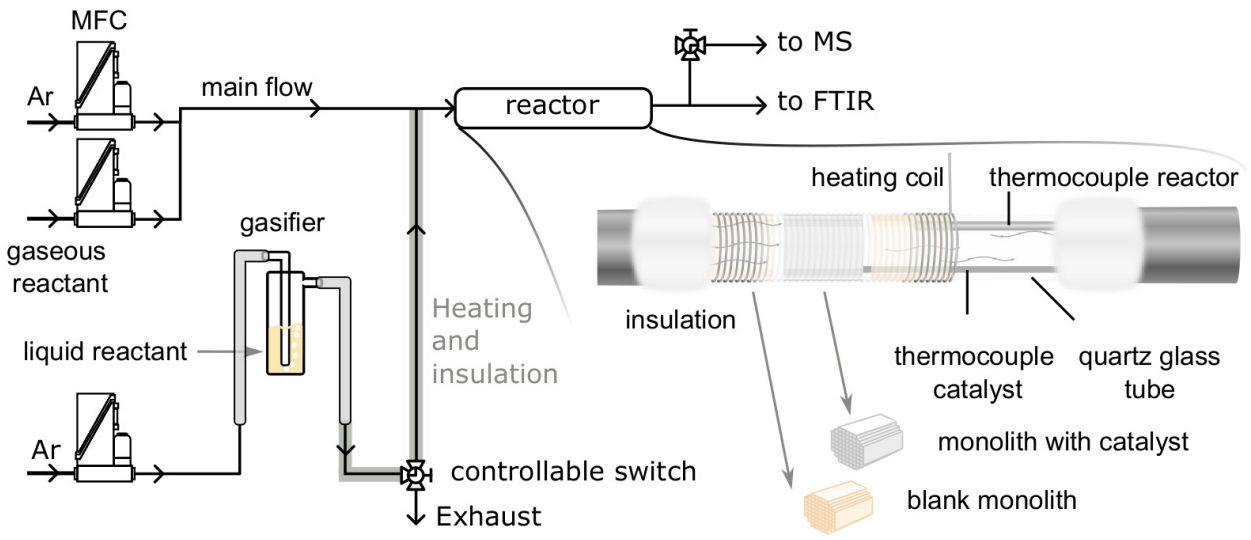

Figure 3.4: Schematic description of the low reactor setup.

3.6 Calibration procedure and on-line analysis

To use a commercial FTIR spectrometer to quantify species present in complex hydrocarbon compositions from biomass-derived model compounds requires a substantial extension of the commercial reference compound library. Many expected species such as water, carbon oxides, alkanes and even BTX are included, but organic molecules derived from biomass are not readily available. To enrich the library's calibration files, which consist of IR spectra and the corresponding compound concentrations, systematic measurements of the missing compounds' spectra of different concentrations are carried out.

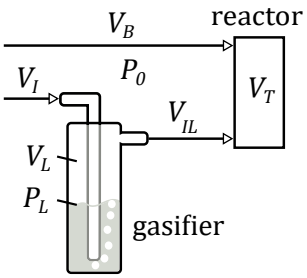

Figure 3.5: Volume flows using the gasifier setup.

V_I : Volume of the inlet flow rate of the carrier gas before going through the gasifier.
V_{IL} : $= V_I + V_L$ Volume of the combined flow rate after the gasifier.
V_L : Volume of the vaporized liquid reactant.
V_B : Volume of the balance gas.
V_T : $= V_B + V_I$ Volume of the set total flow rate.
V_T : $= V_B + V_I$ Volume of the set total flow rate.
V'_T : $= V_T + V_L$ Volume of the actual total flow rate including the vaporized liquid.
p_L : Vapour pressure of the liquid reactant.
p_0 : atmospheric pressure.
C : Volume concentration of the vaporized liquid reactant.

High purity chemicals are vaporized using the gasifier set up shown in figure 3.5 to produce a gas stream with a defined concentration of the compound. The concentration can be calculated based on the vapour pressure (equation (3.5)) of the liquid reactant and the partial volumes of the carrier gas. The elaboration follows:

The volume of the vaporized liquid (V_L) can be calculated from the vapor pressure (p_L):

$$V_L = \frac{p_L}{p_0} V_{IL} = \frac{p_L}{p_0}(V_I + V_L) \implies V_L = V_I \frac{p_L}{p_0 - p_L} \tag{3.6}$$

The volume concentration of the vaporized liquid (C) is the volume of the vaporized liquid (V_L) divided by the actual total volume

(V_T') and is calculated as in equation (3.7)

$$C = \frac{V_L}{V_T'} = \frac{V_L}{V_T + V_L} = \frac{V_I \frac{p_L}{p_0 - p_L}}{V_T + V_I \frac{p_L}{p_0 - p_L}} = \frac{V_I p_L}{(p_0 - p_L)V_T + V_I p_L} \quad (3.7)$$

For validation reasons and where vapour pressures are not available, the concentrations are calculated based on the mass of the liquid reactant that was vaporized into the gas phase. The mass of the vaporized liquid reactant m_L corresponds to the difference in mass of the gasifier including liquid reactant before and after the vaporization, as in equation (3.8). The feeding of reactant happens in a timescale of hours to vaporize a significant measurable amount. The corresponding spectra are further averaged in intensity to account for small deviations in flow stability. From the mass (m_L) and the molar mass (M_L), the amount of substance (n_L) can be calculated. To calculate the concentration (C), the amount of substance of the carrier gas (n_G) is needed. The latter can be obtained by the ideal gas law equation (3.10), where p_0 is the atmospheric pressure, V is the total volume of the carrier gas at temperature T and R is the ideal gas constant. V corresponds to the volume of the total flow rate f_n multiplied by the time during which the liquid reactant is evaporated.[6] The concentration is finally obtained from equation (3.11).

$$m_L = m_b - m_a \quad (3.8)$$

$$n_L = \frac{m_L}{M_L} \quad (3.9)$$

$$pV = nRT \quad (3.10)$$

6: $f_n = 1500\,\mathrm{mL_n/min}$, with $\mathrm{mL_n}$ under normal conditions at T=273.15 K and p_0=103 125 Pa.

$$C = \frac{n_L}{n_G} = \frac{\frac{m_b - m_a}{M_L}}{\frac{p_0 V}{RT}} \quad (3.11)$$

IR spectra of the stream including the known amount of vaporized liquid reactant are recorded continuously. All spectra are saved and averaged resulting in a good signal to noise ratio and assigned to their corresponding concentrations to create calibration files to supplement the reference compound library. In these calibration files, a primary analysis band for each compound is chosen. This primary analysis band is used to calculate the concentration of a compound in the FTIR analyzers software based on the measured absorption using Classical Least Squares (CLS).[7]

7: For more details, see Paper I.

Results and discussion 4

This chapter will guide the reader through the progress of this research project. The initial challenges of monitoring a complex hydrocarbon product stream with on-line FTIR in a continuous flow reactor and how they are overcome will be discussed. The speciation of conversion products in the catalytic reaction is followed by the calibration of identified species and enrichment of the commercial FTIR library. Complementary mass spectra and validation of the method follows. These findings are the content of Paper I, together with a profound discussion about the importance of on-line analysis.

Subsequently, the developed method is applied to analyze the product streams and reactions using the different zeolite materials as described in table 3.3. Supplemented by *in situ* temperature-programmed desorption experiments using IR spectrometry in diffuse reflectance mode, the first mechanistic conclusions and relations between catalyst structure and their function are drawn, which is summarized in Paper II.

4.1 A complex stream – a complex spectrum

The first challenge encountered when trying to analyze the complex hydrocarbon stream was the speciation of the conversion products in the stream. In the early stage of this work, the available literature helped giving an idea of the manifold of species present during the catalytic conversion of furans over zeolites. A wide range of compounds had been identified, usually by collecting the sample in gas bags and liquid traps before separation by GC and analysis by FID, TCD or MS. [42, 54, 55] Even for model compounds, the HC product distribution is usually quite broad, including several decarbonylation and dehydration products such as carbon oxides, water, alkanes, alkenes as well as aromatics including hetero- and polycycles, such as BTX, indene and naphthalenes. [37, 38, 42] With a first idea of what to expect, these species are generated by a real catalytic experiment. In a catalytic flow reactor equipped with a zeolite catalyst coated on a monolith substrate as described in chapter 3, the liquid reactant is fed into the reactor.[1]

An IR spectrum of the HC stream is presented in figure 4.1. Besides the easily recognized signals of water, CO and CO_2, a complex

1: Initial problems with clogging of the existing controlled evaporation system and too high feed concentrations were finally solved by introducing a gasifier setup.

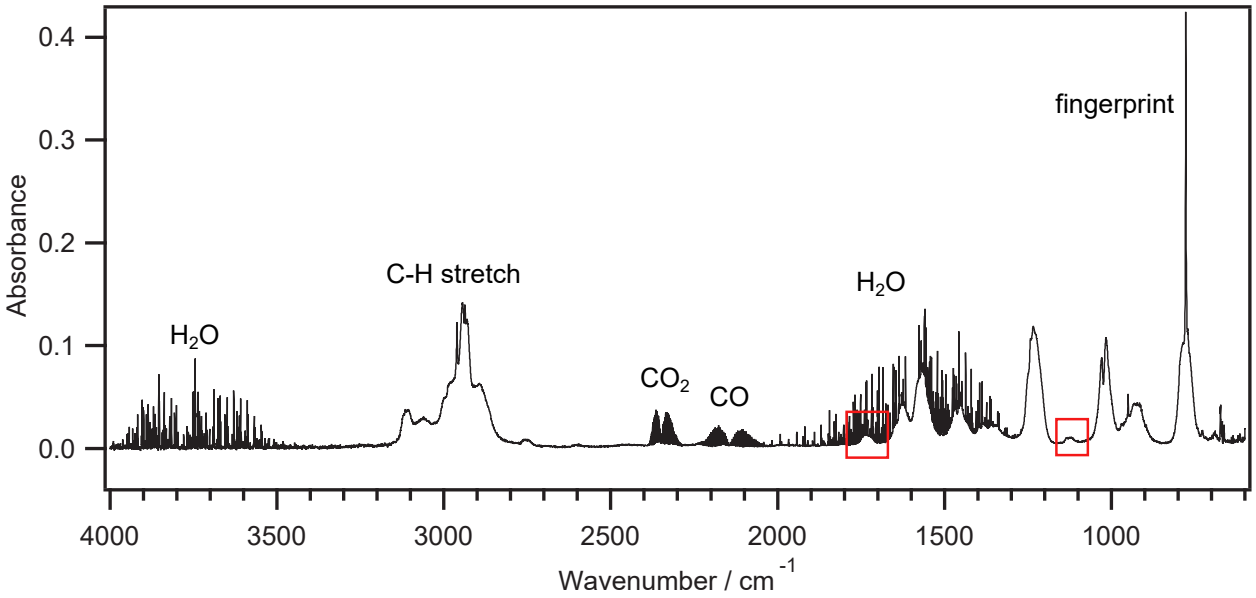

Figure 4.1: IR spectrum of the HC stream after conversion of 2,5-dmf over H-ZSM5 SAR330.

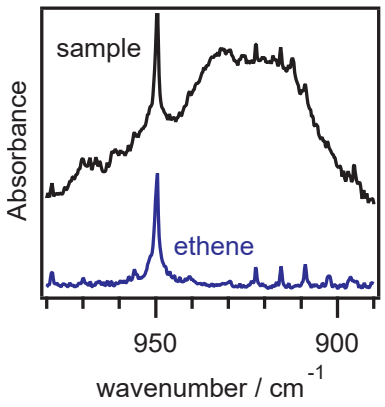

Figure 4.2: Ethene peaks observed in the conversion stream for H-ZSM5 SAR330. Black line: sample spectrum, blue line: reference spectrum.

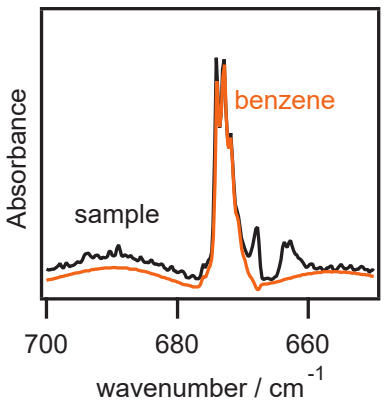

Figure 4.3: Benzene signal observed in the conversion stream for H-ZSM5 SAR330. Black line: sample spectrum, orange line: reference spectrum.

spectrum is observed. A closer look reveals the presence of hydrocarbons, identified by their characteristic absorption bands, which required extensive screening of the sample spectra and matching them to existing reference compounds. Figure 4.2 shows the ethene signal around 950 cm^{-1} compared to that of the sample stream obtained during 2,5-dmf conversion over H-ZSM5 SAR330. For the same material, the benzene signal is presented in figure 4.3.

However, the signal strength of these compounds and thus their concentration is not only dependent on time on stream (TOS) – as we will learn later – but also on the catalytic material and temperature. Figure 4.4 shows the signal of 1,3-butadiene for the H-ZSM5 SAR55 sample, the only one of the tested samples showing selectivity to this product. Methane on the other hand is observed at high temperatures, for example around 500 °C, as shown in figure 4.5.

Even with the available literature at hand, not all species can be identified by their characteristic bands, partly due to the very low concentrations, partly due to overlapping of bands from different compounds. Some remaining bands could not be attributed to any reference compounds. This applies for example to the observed signal between 1140 cm^{-1} to 1110 cm^{-1}, highlighted in red in figure 4.1. The band between 1760 cm^{-1} to 1700 cm^{-1} was attributed to the C=O stretch vibration of a ketone, a species that was not previously reported as a conversion product in CFP studies based on furanic model compounds. 2,5-hexanedione, a side product that has been observed due to hydrolysis of 2,5-dmf in DACD experiments, [30] matches the ketone group frequency but finally, this signal can not be assigned to 2,5-hexanedione, because its

pronounced bands at 1380 cm^{-1} to 1340 cm^{-1} and 1180 cm^{-1} to 1140 cm^{-1} cannot be found in the sample spectra and its origin remained unclear. Another band with a peak at 925 cm^{-1} that is sometimes detected but not shown here could not be identified either.

To reveal these unknown species, a sample of the diluted stream was adsorbed onto multisorbent tubes in a separate experiment. The tubes are columns for further separation via gas chromatography and analysis with mass spectrometry. The collected species represent only the "heavy" fraction of the conversion stream such that light gases, *e.g.*, ethene, CO and CO_2, are excluded. A summary of the GC–MS analysis is shown in table 4.1. Unconverted reactant 2,5-dmf is the biggest fraction found in the sample with about 75% (as toluene equivalents). The second largest signal is from the reactants isomer 2,4-dimethylfuran (2,4-dmf), which has so far not been reported in similar experiments. Other isomerization products of the reactant including 2-methyl-2-cyclopenten-1-one and 3-methyl-2-cyclopenten-1-one are also identified as conversion products. Some expected products such as BTX, indene and naphthalenes are found in the sample. 6% of the total sample are benzene molecules. Further, other heavier aromatics and polycycles like indene and naphthalenes are present. Even some 5- and 7-membered C-cycles are identified as 3-methylene-cyclopentene, 5-methylcyclopenta-1,3-diene and 1,3,5-cycloheptatriene.

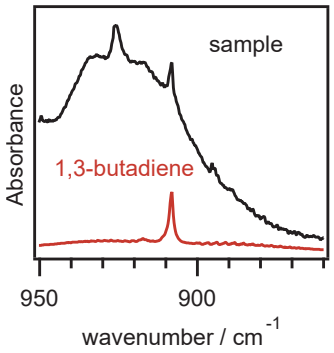

Figure 4.4: 1,3-butadiene signal observed in the conversion stream for H-ZSM5 SAR55.

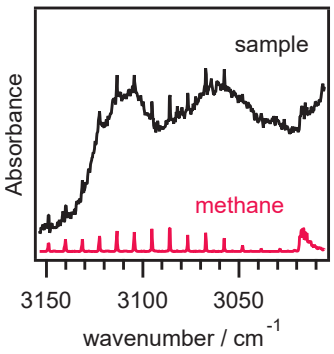

Figure 4.5: Methane peaks observed in the conversion stream for H-BEA SAR38 at 500 °C.

Table 4.1: "Heavy" fraction molecules during 2,5-DMF conversion over a zeolite (ZSM5-SAR330) identified with GC–MS analysis.

Name	formula	mass ($\frac{g}{mol}$)	toluene eq. (%)
Furans			
2,5-dimethylfuran	C_8H_8O	96	75
2,4-dimethylfuran	C_8H_8O	96	14
2-methylfuran	C_5H_6O	82	0.7
2,3,5-trimethylfuran	$C_7H_{10}O$	110	0.1
BTX			
Benzene	C_6H_6	78	6.0
Toluene	C_7H_8	92	0.9
Xylenes	C_8H_{10}	106	0.2
C_5-rings			
2-methyl-2-cyclopenten-1-one	C_6H_8O	96	0.7
3-methyl-2-cyclopenten-1-one	C_6H_8O	96	0.2
3-methylene-cyclopentene	C_6H_8	80	0.2
5-methylcyclopenta-1,3-diene	C_6H_8	80	1.0
C_7+-rings and polycyclic compounds			
1,3,5-cycloheptatriene	C_7H_8	92	1.0
Indene	C_9H_8	116	0.2
Naphthalene	$C_{10}H_8$	128	0.1
1-methylnaphthalene	$C_{11}H_{10}$	142	0.1
1,5-dimethylnaphthalene	$C_{12}H_{12}$	156	0.1

4.2 Calibration for the infrared spectroscopy

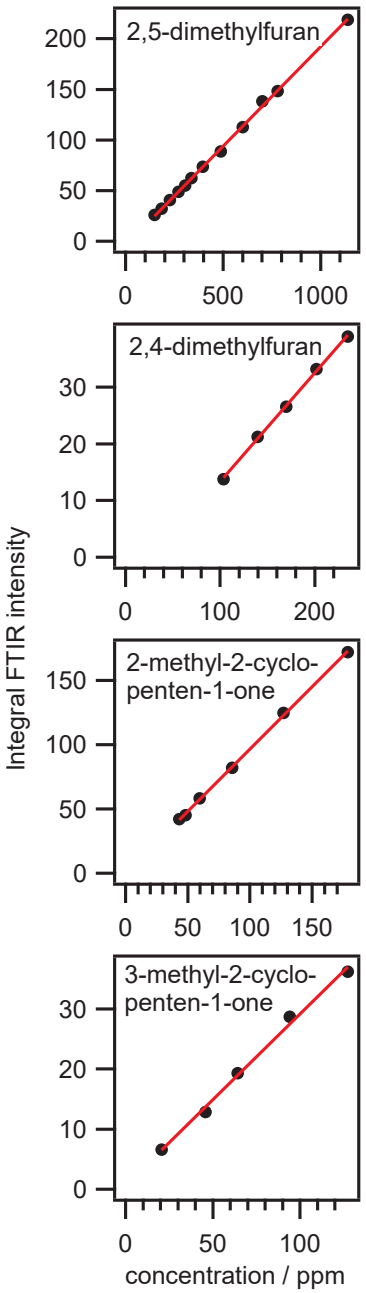

Figure 4.6: Absorbance vs gas concentration and its linear fit for 2,5-dmf, 2,4-dmf and 2- and 3-methyl-2-cyclopenten-1-one.

Now that most species are identified, the existing reference compound library of the FTIR instrument requires an expansion. Although many common inorganic and organic compounds are included, biomass-derived species, their isomers and some conversion products that are of special interest to this work are not available. These range from the various furans to the aforementioned isomeres like 2- and 3-methyl-2-cyclopenten-1-one. After acquisition of the pure reference chemicals, systematic calibrations for these compounds are carried out. This happens through a process of feeding a defined gas concentration of the sample into the FTIR cell and measurement of the corresponding absorption spectra. In the case of 2,4-dimethylfuran and 2-methyl-2-cyclopenten-1-one, the very first mid-IR spectra are reported, to our best knowledge, in Paper I. In a series of calibration experiments, the concentrations are assigned to their corresponding absorption spectra. According to the *Beer-Lambert* law (equation (3.3)), a linear correlation between absorption and concentration is expected. This behaviour is well demonstrated in figure 4.6 for 2,5-dmf, 2,4-dmf and 2- and 3-methyl-2-cyclopenten-1-one.

The theoretical concentration in the gas stream based on the sample's vapor pressure (equation (3.7)) is compared to the concentration based on the measured mass difference of the liquid (equation (3.11)) in the gasifier before and after the sampling. First of all, a linear correlation is expected between the concentration and the flow rate of the carrier gas through the gasifier. Secondly, the mass based concentration should have the same value as the vapor pressure based concentration for a given flow rate under the assumption, that the gas is saturated with the liquid reactant. Both assumptions are verified by the presentation in figure 4.7. Linear correlation is observed, as well as matching values for the given data points. Small deviations in the mass based concentration are readily explained by an initial overshoot of the MFC feeding the carrier gas, leading to slightly higher concentrations, but do not have a significant influence on the overall accuracy.

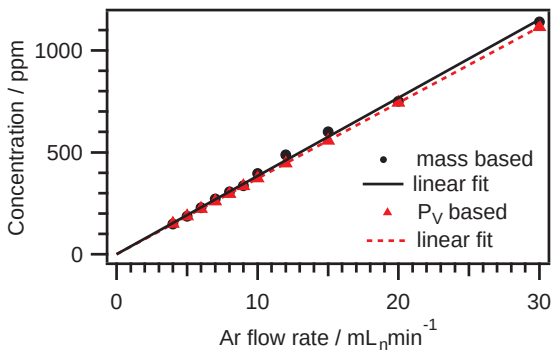

Figure 4.7: Validation of the feed concentration: The mass-based concentration and the theoretical gas concentration based on the vapour pressure P_V as a dependency of the flow rate of the carrier gas show a good match.

4.3 Complementary mass spectrometry

Another investigation addresses the question of how IMR-MS can complement the FTIR analysis. Firstly, mass spectrometry can help where gas concentrations are too low to be accurately followed by FTIR. This is for example the case for xylenes. The higher sensitivity of mass spectrometry allows the analysis of xylenes in the stream at m/z 106. One disadvantage is that the three xylenes can not be distinguished this way. Secondly, species that are of minor interest and can not be easily added to the FTIR library such as 1,3,5-cycloheptatriene, can be tracked on their specific m/z when no cross-talking to other molecules is expected. Lastly, MS is used as a second analytical technique to validate the results of the FTIR method. This is extremely valuable when FTIR detects a false positive, a common problem when analyzing complex HC streams, [56] or overestimates the concentration of a present compound because there is an unidentified absorber with a similar absorption band. Figure 4.8 depicts the signal match of FTIR and IMR-MS when using Hg as an ionizer. In the case of ethene, the signals show a perfect match when following the concentration of the compound in a real catalytic experiment during two pulses of 2,5-dmf. This is because no other specimen gives a signal at m/z 27, meaning there is no cross-talk. In contrast, the signal of 2,5-dmf observed by IR is slightly lower than the one observed by MS with increasing time on stream. This is explained by an increasing isomerization of 2,5-dmf to 2,4-dmf and 2- and 3-methyl-2-cyclopenten-1-one.[2] All of these compounds are detected as well at m/z 96, causing a cross-talk between the four analytes.

2: For a more detailed discussion about this see section 4.5 Isomers.

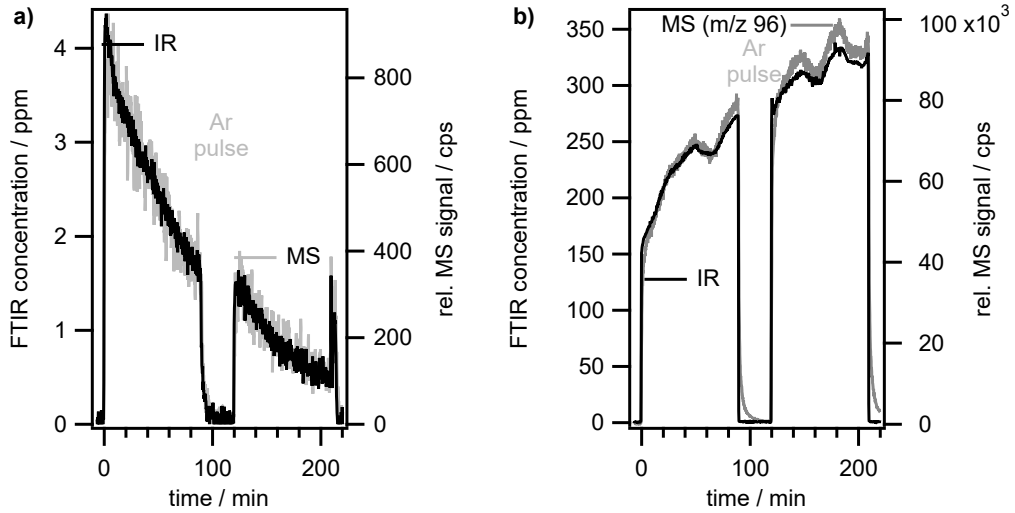

Figure 4.8: Comparison of FTIR and MS: Signal match of IR and MS for **a)** ethene (m/z 27) and **b)** 2,5-dimethylfuran (m/z 96).

It was then interesting to explore if IMR-MS can be utilized to distinguish these four structural isomers. The fragmentation of a

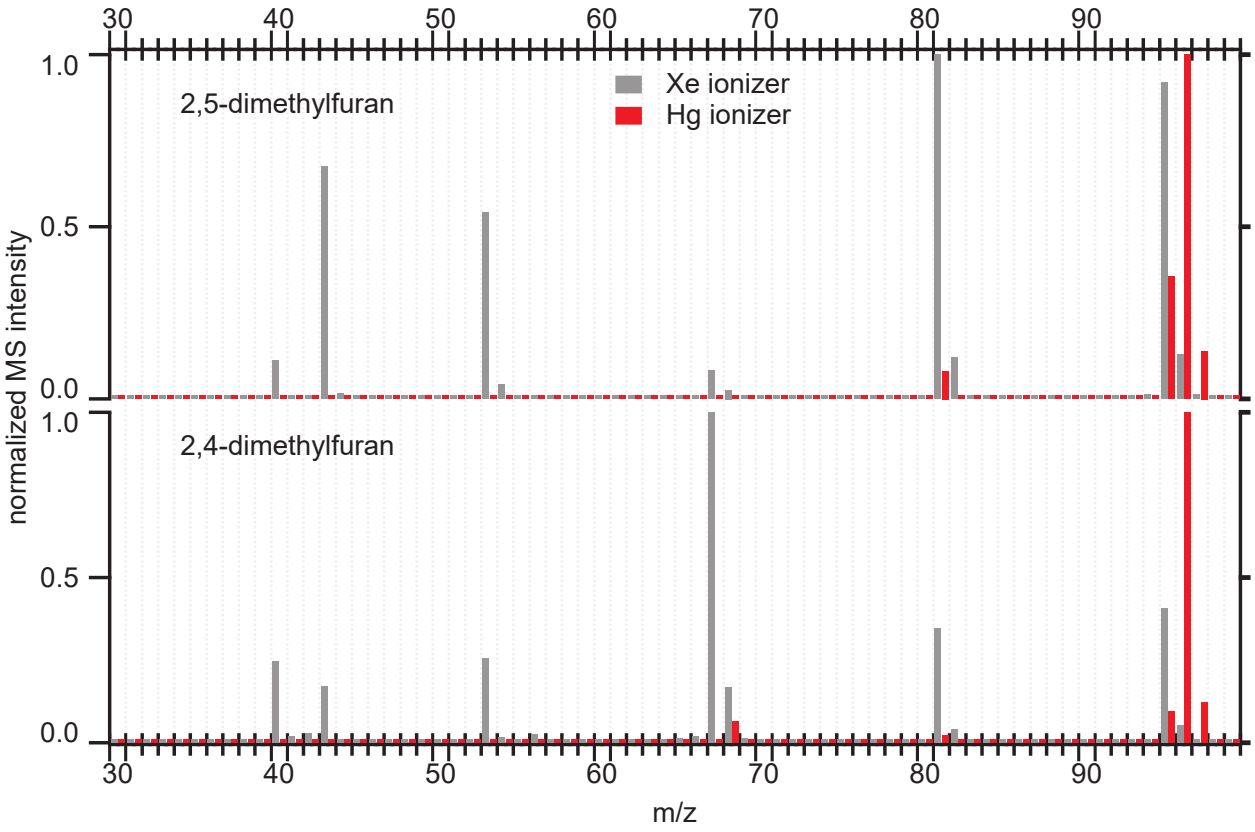

Figure 4.9: Mass spectra of 2,5-dmf and 2,4-dmf using ion-molecule reaction ionization with Hg and Xe.

molecule during ionization is dependent on the energy potential. Using an ion source with lower energy potential, the number of observed fragments is expected to be less. This is clearly visible in figure 4.9 when comparing Hg (ionization potential of 10.44 eV) with Xe (ionization potential 12.13 eV) as ionizers.[3] The spectra obtained with Hg, show much less fragmentation compared to the ones obtained with Xe as ionizing gas. Looking at the signals produced by Hg, only 2,4-dimethylfuran shows a peak at m/z 68, but not 2,5-dimethylfuran. Due to their different structure, and thus stability, the fragmentation pattern using the same ionizer is also different. This can be exploited to distinguish 2,5-dimethylfuran from its structural isomers. The spectra for 2- and 3-methyl-2-cyclopenten-1-one are discussed in more detail in Paper I.

3: see also table 3.2

A careful selection of primary analysis bands for the molecules in the complex hydrocarbon stream was necessary to minimize false positives and cross-talk between different analytes. The selection of m/z and the ionizer in the MS-method was chosen to minimize cross talk and to complement the FTIR method wherever possible, although possibilities for further extension and improvement remain. The combination of the two analytical techniques finally led to a wide range of hydrocarbons and other light gases being analyzed on-line and simultaneously without the need for separation as presented in table 4.2.

Compound	Formula	m/z	IR band (cm^{-1})
Other rings			
2-methylnaphthalene	$C_{11}H_{10}$	142	
Naphthalene	$C_{10}H_8$	128	758.62 – 807.32
2-methyl-2-cyclopentenone	C_8H_8O	(96), 68	1668.88 – 1809.90
3-methyl-2-cyclopentenone	C_8H_8O	(96), 68	1701.42 – 1811.83
Furans			
2,5-dimethylfuran	C_8H_8O	96, (81)	1168.43 – 1282.69
2,4-dimethylfuran	C_8H_8O	(96), 68	1074.17 – 1174.70
2-methylfuran	C_7H_6O	(81)	1117.57 – 1176.87
BTX			
Benzene	C_6H_6	78	606.51 – 726.80
Toluene	C_7H_8	92	689.44 – 769.95
o-xylene	C_8H_{10}	106	702.45 – 779.59
p-xylene	C_8H_{10}	106	735.32 – 867.92
Olefins			
Ethene	C_2H_4	(28), 27	900.12 – 1000.16
Propene	C_3H_6	42, (41)	900.61 – 1019.69
1,3-butadiene	C_4H_8	(54)	2698.93 – 2822.36
C_1			
Methane	CH_4	-	3000.25 – 3176.23
Carbonmonoxide	CO	28	2146.16 – 2159.90
Carbondioxide	CO_2	44	2223.57 – 2280.94
Formaldehyde	CH_2O	(30)	2698.93 – 2822.36
Water	H_2O	18	1416.97 – 1502.31

Table 4.2: Molecules analyzed simultaneously in the complex gas stream with their chosen m/z and primary IR analysis band.

4.4 Applying the on-line analysis to catalytic experiments

With a working method, on-line FTIR-MS analysis was applied to real catalytic experiments. The four catalytic materials (table 3.3) were exposed to a sequence of two pulses of 2,5-dimethylfuran at 500 °C and one pulse at 400 °C and 300 °C as schematically depicted in figure 4.10. Before and between every temperature step, the catalyst was calcined in 20% oxygen to remove any carbon depositions which lead to catalyst deactivation.

The FTIR data for such a catalytic experiment is shown as a contour plot of the FTIR intensity at the given wavenumber exemplary for the H-BEA sample in figure 4.11.

From this data, concentration profiles can be constructed for all analyzed molecules. Overall, the carbon balance[4] exemplified for the zeolite BEA sample closes at 89, 93 and 97 % at 500, 400 and 300 °C, respectively. This is comparable to GC–MS analysis of similar CFP processes .[37] It would be beyond the scope of this thesis to show all specimens, but a few concentration profiles are discussed to exemplify the complexity of this topic. For full coverage, the reader is referred to Paper II. A summary is given here, especially covering the most interesting selectivity changes towards the structural isomers of the reactants.

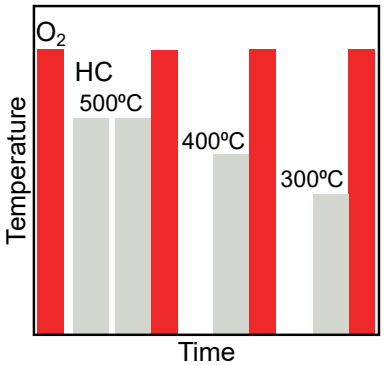

Figure 4.10: Experiment sequence: Catalyst calcination under 20% oxygen at 700 °C, HC pulses of 2,5-dmf at 500 °C, 400 °C and 300 °C.

4: Carbon balance here means the amount of C atoms leaving the reactor divided by the amount of Carbon entering the reactor. This means that most of the stream composition is identified and quantified.

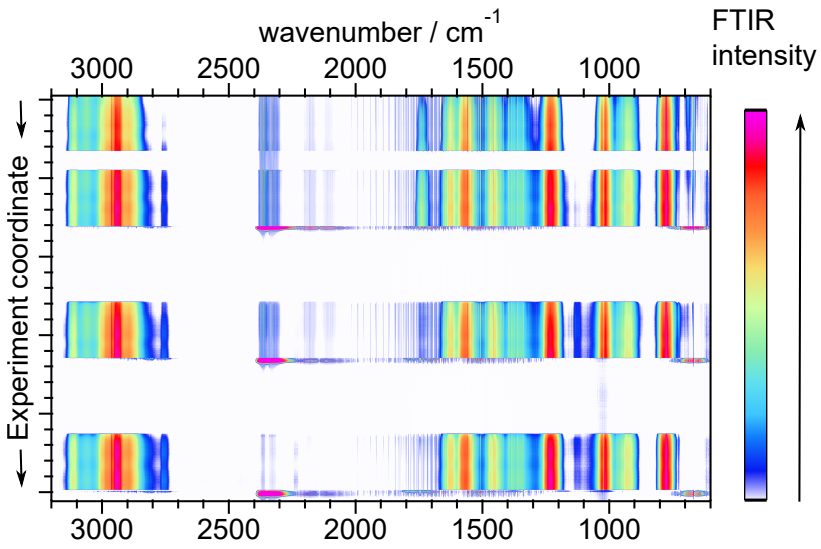

Figure 4.11: Contour plot of the FTIR intensity for the given wavenumbers during the catalytic experiment for pulses of 2,5-dmf at 500 °C, 400 °C and 300 °C.

Olefins

Olefins are among the catalytic conversion products of furanic compounds over zeolites. [38, 42, 55]

1,3-butadiene is almost exclusively formed over the more acidic H-ZSM5 SAR55 especially at 500 °C, while it is hardly observed over the other three examined samples. While H-ZSM5 SAR330 is less acidic due to its lower Al content, the ion exchange of Cu decreases acidity for Cu-ZSM5, indicating that acidity plays a role in 1,3-butadiene production. The H-BEA sample shows very low selectivity to 1,3-butadiene which might be further explained by its different structure and thus shape selectivity. Out of the four samples, H-ZSM5 SAR330 shows the highest selectivity towards both propene (figure 4.12) and ethene[5], followed by H-BEA SAR38. As a general trend for all samples, the selectivity towards propene is the highest at 400 °C, whereas for ethene it is at 500 °C. At 300 °C very low or no activity is observed for either of the compounds. For all samples, the selectivity towards propene and ethene decreases with time on stream, which is attributed to the increasing deactivation of certain active sites.

Aromatics

Looking at the benzene signal in figure 4.12 the Cu-ZSM5 sample shows significantly higher initial selectivity towards benzene at 500 °C but experiences a faster deactivation compared to H-ZSM-5 SAR330, which shows the second-highest selectivity with a slower decline in benzene formation. The initial higher activity towards benzene over the Cu-ZSM-5 sample can be explained by its lower acidity which promotes benzene selectivity and the presence of Cu sites active for benzene formation. An obvious trend shows

5: not shown here, see Paper II

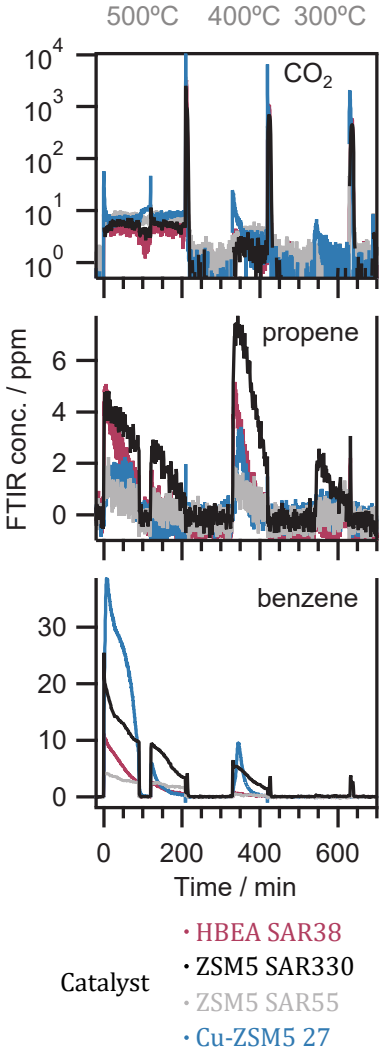

Figure 4.12: Concentration profiles of CO_2, propene and benzene.

that selectivity towards benzene is higher at elevated temperature, which was also reported previously using furan [42] and 2,5-dmf [38] as feedstocks.

The highest selectivity towards toluene is observed for H-ZSM5 SAR330 and the H-BEA sample at 500 °C and 400 °C (not shown here, see Paper II). Despite the same trend for xylenes regarding temperatures, the selectivity is in general very low for the CFP of furanic compounds. [37–39, 42, 43, 55] Regarding the on-line analysis method, xylenes are qualitatively tracked by IMR-MS, because concentrations detected with FTIR are below 2 ppm.

Again, for all samples, the BTX selectivity decreases with TOS indicating deactivation of the catalysts.

Isomers

2,4-dimethylfuran In contrast to previous studies, the formation of 2,4-dmf has been observed during 2,5-dmf conversion for the first time. As a constitutional isomer of 2,5-dmf, the break of a bond is necessary to form 2,4-dmf from 2,5-dmf via isomerization, which is called a methyl shift. The hypothesis of a methyl-shift caused by a combination of the BAS and the shape selectivity of the zeolite catalyst is supported by a similar, already known phenomenon: the isomerization of m-xylene to p-xylene in ZSM-5. [20] The concentration profile of 2,4-dmf is displayed in figure 4.13 showing highest selectivity at 400 °C for all samples. For the H-ZSM-5 SAR55 and SAR330 sample, the concentration increases with time on stream. This indicates coking of the catalyst and thus blocking of specific active sites increases selectivity to 2,4-dmf. The isomerization is expected to appear in the zeolites' pores due to their shape selectivity. For zeolite beta with a larger pore size and thus smaller sterical pressure [19], a lower selectivity towards 2,4-dmf is detected, supporting the above hypothesis. Furthermore, demethylation to 2-methylfuran and methylation to 2,3,5-trimethylfuran were found by the GC–MS analysis, further supporting this mechanism.[6] The Cu-ZSM5 sample shows a lower selectivity which is likely explained by Cu blocking active BAS sites and thus decreased amount of acid sites. The availability of strong acid sites seems necessary for this isomerization. This observation opens the opportunity for the more selective production of the not easily accessible 2,4-dimethylfuran from inexpensive 2,5-dmf. As a minor side-product of wooden biomass conversion 2,4-dmf has been detected before. [58] It has even been described to play a role in the decomposition of 2,5-dmf [59].

2- and 3-methyl-2-cyclopentenone None of these two constitutional isomers has been previously described during the CFP of

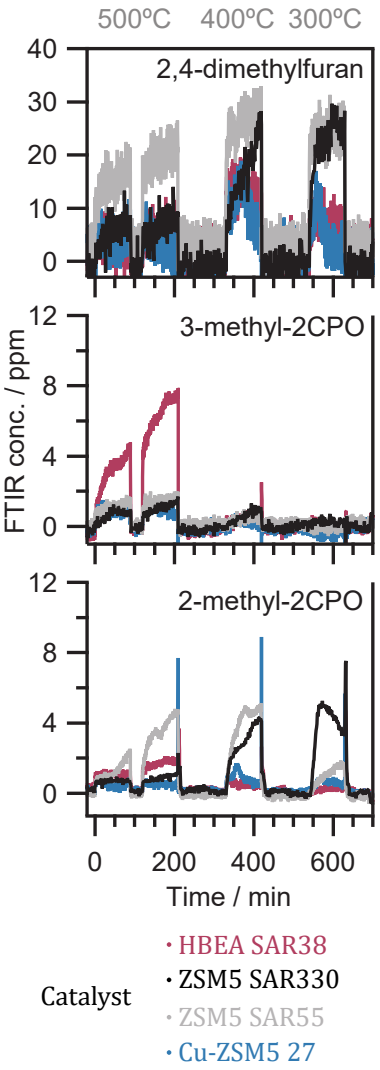

Figure 4.13: Concentration profiles of 2,4-dmf, 2- and 3-methyl-2-cyclopenten-1-one.

6: Methylation of furan to 2-methylfuran was reported by Gilbert *et al.* [57]

2,5-dmf. However, 3-methyl-2-cyclopentenone has been observed during the DACD experiments of 2,5-dmf to p-xylene in the solvated phase. [60] 2-methyl-2-cyclopenten-1-one was found during CFP of agricultural waste [58] and other pyrolysis vapours [61–63].

The highest selectivity towards 3-methyl-2-cyclopentenone at 500 °C is shown by the H-BEA sample, while not much of this product is detected at lower temperatures. MFI structured samples seem to favour the formation of 2-methyl-2-cyclopentenone, at 400 °C by both of the H-ZSM5 samples and at 300 °C by the H-ZSM5 SAR330 sample. The Cu-ZSM5 sample has the lowest selectivity, which can be explained by the suppression of ketone formation by Cu, possibly through blocking other important active sites. The observation of 3-methyl-2-cyclopentenone as a side product of 2,5-dmf under DACD conditions in the solvated phase has been reported in previous studies. Its formation is explained by initial hydrolysis of 2,5-dmf to 2,5-hexanedione and subsequent dehydration and intramolecular aldol condensation to 3-methyl-2-cyclopentenone. [64, 65]

However, in this work, as well as in other CFP studies of 2,5-dmf, no 2,5-hexanedione was found. Possible factors are the absence of solvent as well as the difference in pressure (50 bar vs atmospheric) and temperature (250 vs 300 °C to 500 °C). Many questions in the reaction pathway and the cause of this behaviour remain and require further attention.

4.5 Mechanistic insights

Although the DACD reaction seems to be a theoretical possible pathway, it might not be the preferred route under CFP conditions [38] as opposed to those under high pressure in batch reactors, where high selectivity to *p*-xylene can be achieved using unpolar solvents [33].

Instead, BTX are formed from the olefin pool. The presence of 1,2-propadiene[7] has been reported for the conversion of furan and it has been postulated to play a role during aromatization. [42, 55] In this work, the presence of 1,2-propadiene in the product stream during 2,5-dmf conversion can not be confirmed. The aromatization must thus be originating from the remaining olefins, namely ethene, propene and 1,3-butadiene.

7: $H_2C{=}C{=}CH_2$

The relative signal intensity of propene has a correlation with the toluene signal, while ethene formation correlates with benzene production. This is an indication that aromatics production is dependent on olefins formed directly from 2,5-dmf. Hence, the

aromatization could be caused by olefins. [66] As an example, toluene could be made of two C_2 and one C_3 building block, incorporating one propene molecule, which delivers the CH_3 group.

Temperature programmed desorption

The correlation of aromatic product depending on olefin presence leads to the investigation of a temperature programmed desorption experiment. [8] As shown in figure 4.14, the desorption signals below 100 °C are assigned to unreacted 2,5-dmf. At higher temperatures, the desorption of olefins and BTX is observed. The maximum of the desorption profile for each species was evaluated to obtain the temperature of maximum desorption $T_{\text{max Des}}$.

8: The H-BEA powder sample was saturated with 2,5-dmf and the temperature was increased stepwise while tracking conversion products with IMR-MS.

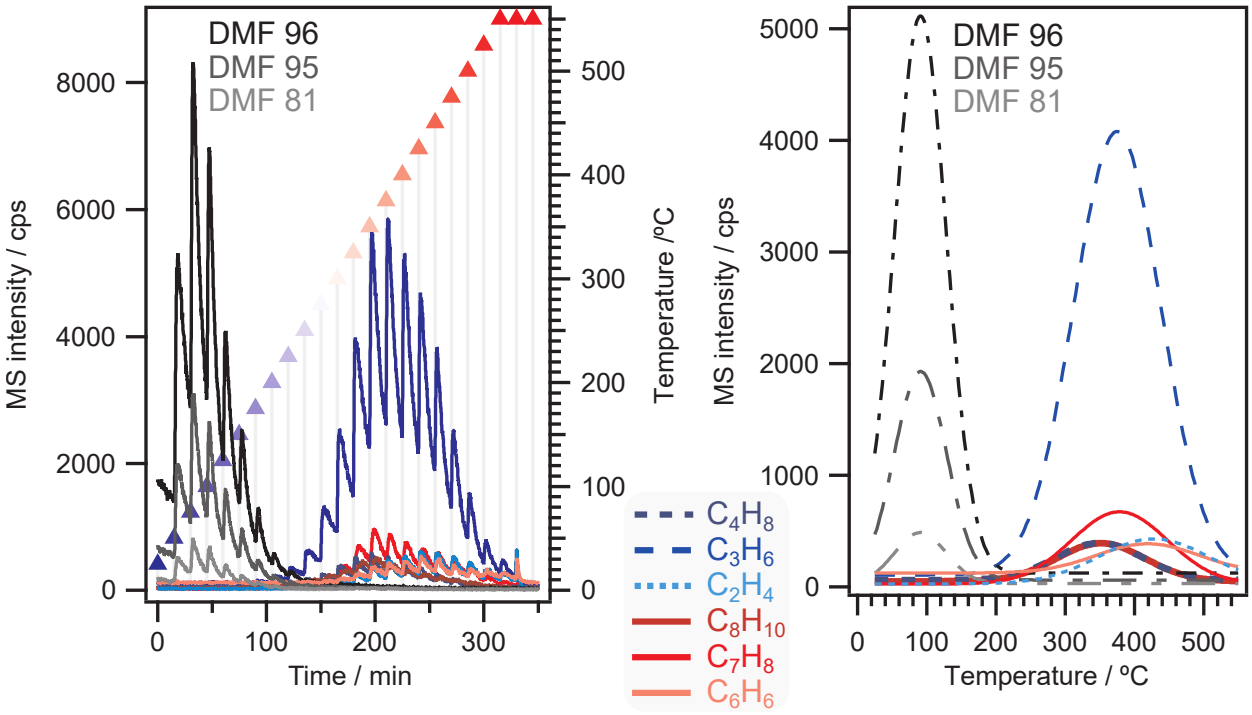

Figure 4.14: Temperature programmed desorption of 2,5-dmf and its olefinic and aromatic conversion products.

In this experiment, the desorption of a C_4H_8 species, possibly butene, is detected at a similar temperature as xylene around 350 °C. Toluene correlates with propene around 380 °C while at the highest temperatures desorption of benzene and ethene is recorded. (table 4.3).

Although this is no evidence, the correlation in $T_{\text{max. Des.}}$ between certain olefins and certain aromatics supports the hypothesis of the direct aromatization from olefins. This assumption is based on the thought that certain olefins have to be available for the formation of aromatics, while at the same time no desorption of 2,5-dmf is

Table 4.3: Desorption maxima of 2,5-dmf, BTX and olefins.

Species	$T_{\text{max Des}}$ /°C
2,5-dmf	91
xylene	352
toluene	379
benzene	418
butene	349
propene	376
ethene	429

detected. However, DACD remains a possible pathway, at least for the formation of *p*-xylene from 2,5-dmf and ethene.

In situ infrared spectroscopy

Uslamin *et al.* found that unsubstituted furan undergoes decarbonylation to CO_x, while methylated furans are preferably deoxygenated by dehydration. [38] From the on-line analysis in this thesis we learn about differences in selectivity towards CO, CO_2 and H_2O during the conversion of 2,5-dmf even the different catalyst samples. In general, CO, CO_2 and H_2O formation are lower at lower temperatures, which is related to lower 2,5-dmf conversion at lower temperatures. The H-BEA sample facilitates dehydration over decarbonylation, showing the lowest selectivity trend towards CO_x. The H-ZSM5 SAR55 and SAR330 samples both show higher decarbonylation activity than H-BEA SAR38. Lastly, the Cu-ZSM5 has very high initial CO_x production at all temperatures, which quickly declines and is fundamentally different than for the other three samples.[9] This required further investigation. To gain further knowledge about surface species when 2,5-dmf interacts with the catalyst, temperature programmed *in situ* IR experiments are carried out. Discussing all observations from the information-rich DRIFT spectra would be far beyond the scope of this thesis and the reader is, therefore, referred to Paper II. Nevertheless, some important aspects are discussed here based on temperature programmed experiments with the powderd Cu-ZSM5 and H-BEA sample. In these experiments a background of the calcined sample is taken at 25 °C before the sample was saturated with 2,5-dmf. All spectra shown are background substracted difference spectra.

9: Compare also figure 4.12 and Paper II.

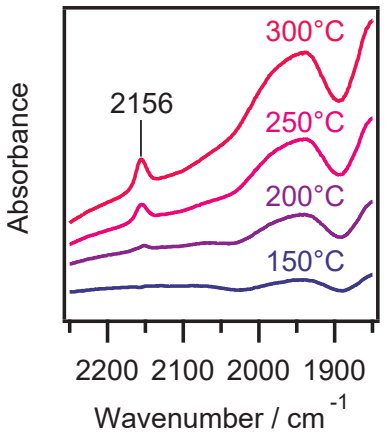

Figure 4.15: Observation of C=O stretch vibration on Cu at 2156 cm^{-1} in a DRIFTS experiment. Difference spectra, background at 25 °C.

10: ν[Cu^+–CO]

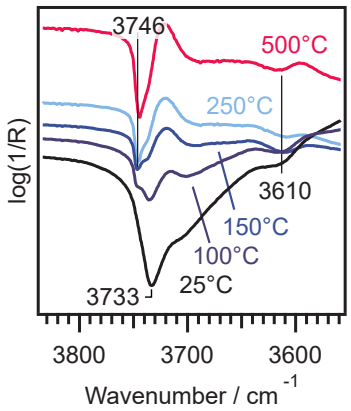

Figure 4.16: The O-H stretching region during a temperature programmed DRIFTS experiment with 2,5-dmf and H-BEA. Difference spectra, background at 25 °C.

Preoxidation of Cu

It is found that CO_x is favoured in the first minutes of the conversion, while hydrocarbons experience their peak after the rapid decline of the CO_x signal. This is explained by the preoxidation of Cu during the oxidative treatment. Cu-centres function as oxygen storage. That means, the Cu-species in the zeolite are pre oxidised and can thus act as an oxidation catalyst of the carbon-rich reactant. [67] Further, a pronounced band is found at 2156 cm^{-1} during temperature programmed *in situ* IR experiments as displayed in figure 4.15. This band is recorded for temperatures ≥180 °C and assigned to C=O stretching vibrations[10] from CO on Cu-species. [52, 68] This gives further evidence to either a decarbonylation pathway or metal-assisted oxidation of HC.

Hydrocarbon species

Figure 4.16 shows an important wavenumber range for zeolite materials. In the case of the H-BEA sample, the peak centred at

around 3733 cm^{-1} is attributed to internal silanols and its neighbour at 3746 cm^{-1} to external silanols. [69, 70] Moreover, the band at 3610 cm^{-1} is assigned to strongly acidic bridged hydroxyl groups (BAS). [71] This leads to the conclusion that upon 2,5-dmf adsorption onto the zeolite, interaction of 2,5-dmf with the internal silanol and BAS is happening. With increasing temperature, the interaction with the internal silanol disappears, while interactions of the same or other species with external silanol and BAS remain.

The C-H stretching region presented in figure 4.17 shows many bands at different wavenumbers. It is clear, that the initial peaks from 2,5-dmf adsorption (e.g. 3007 cm^{-1} and 2910 cm^{-1}, assigned to aromatic C=C-H stretch and alkyl C-H stretch) are changing when the temperature increases. This complex region shows evidence of the formation of other hydrocarbons on the catalyst surface. For a full understanding, further in-depth study and possibly deconvolution of overlapping signals is necessary.

Finally, in figure 4.18 a strong band at 1713 cm^{-1} indicates a C=O vibration, that is quickly decreasing in strength along temperature increase until complete disappearance at 175 °C. Since a C=O stretching vibration is expected for a ketone but not for an O-heterocycle whose C-O-C vibration is usually at lower wavenumbers, the hypothesis stands, that 2,5-dmf is prone to ring opening and formation of a C=O group when adsorbed onto the zeolite. Lastly, two bands at 1633 cm^{-1} and 1655 cm^{-1} are emerging above 100 °C indicating the appearance of new C=C vibrations.

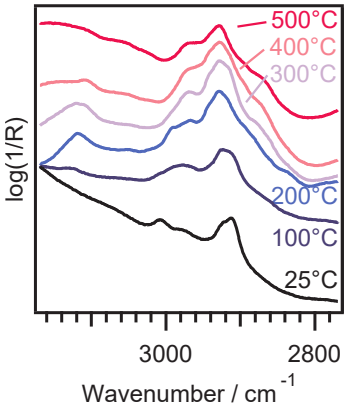

Figure 4.17: The C-H stretch region during a temperature programmed DRIFTS experiment with 2,5-dmf and H-BEA. Difference spectra, background at 25 °C.

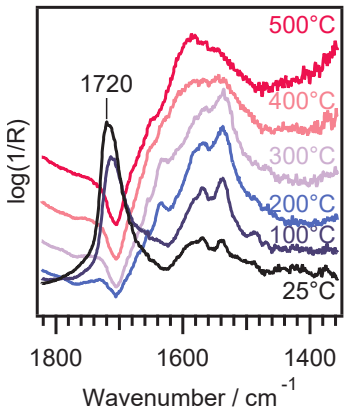

Figure 4.18: The region between 1800 cm^{-1} to 1400 cm^{-1} during a temperature-programmed DRIFTS experiment with 2,5-dmf and H-BEA. Difference spectra, background at 25 °C.

Conclusions and future work

5

A method to study the conversion of furans over acid-based catalyst materials has been developed using FTIR spectroscopy and IMR-mass spectrometry. For this purpose, a complex hydrocarbon stream obtained during the 2,5-dmf conversion was analyzed extensively by GC–MS, infrared spectroscopy and IMR–MS. Several absorption spectra and their concentrations were calibrated as reference compounds to extend the existing FTIR library. In this regard, the first mid-infrared spectra of 2,4-dimethylfuran and 2-methyl-2-cyclopenten-1-one are reported in Paper I. Furthermore, mass spectra using ionization sources with different ion potentials for various chemicals are reported. It is shown that the two analytical techniques complement and validate each other, resulting in a reliable method for online analysis of complex hydrocarbon streams in the gas phase, which is free from molecular separation prio to analysis. The time resolution is increased to at least 4 min^{-1}, outperforming separation based analysis methods which can at best operate at a several-minute scale. This allows for experiments in transient response mode as well as high automation. The carbon balance is found to be around 90% which is comparable to existing studies.

This method is applied to catalytic experiments using four different zeolitic materials. The selected samples represent two different framework structures and different acidity. One sample has metal-based active sites prepared by Cu-ion exchange. The different catalytic materials show distinct variations in product selectivity. Beside known processes like cracking of 2,5-dmf to olefins and formation of aromatics, it is found that isomerization reactions play an important role when operating in flow reactor conditions with monolith samples. In CFP conditions the selectivity towards desirable aromatics, especially *p*-xylene is low. Possible reaction pathways postulated in literature have limited evidence and little focus on studying reaction mechanisms. To illuminate the pathways to formation of the different products, *in situ* infrared spectroscopy and temperature programmed desorption experiments are carried out. More in-depth studies are necessary to understand the scope and complexity when upgrading bio-based molecules to hydrocarbons important to our existing industrial infrastructure.

Although the DACD approach promises high selectivity towards *p*-xylene, the reaction conditions of high pressure, long reaction duration and mixed solvated phase are unfavourable for large-scale production. So far it seems that no DACD reaction takes place under

CFP conditions. However, the knowledge from DACD studies and advanced analysis methods can be used to design better catalysts even for CFP of biomass and its model compounds.

Future outlook

The decrease in selectivity towards olefins and aromatics at the coincident increase in isomerization leads to the speculation that isomerization and deactivation of specific active sites are linked.

It should be investigated if DACD can be achieved under the flow reactor conditions. One possibility might be the spatial separation of active sites for example by having two different catalysts in a row. The first sample features Lewis acid sites that are supposed to catalyse DA cycloaddition while a second BAS catalyst is responsible for the dehydration of the cycloadduct.

Furthermore, the effect of weakened acidity (as opposed to fewer acid sites, *aka* Si/Al ratio) can be tested by using zeotypes, such as Fe-silicalite.

Finally, the on-line analysis offers the possibility for pulsing experiments, such as that one reactant (the diene or dienephile) can be adsorbed to the catalyst prior to a pulse of the other.

Acknowledgements 6

This research was funded by the Swedish Research Council for Environment, Agricultural Sciences and Spatial Planning (Formas) [No. 2017-00420].

I want to thank my main supervisor Per-Anders Carlsson for your guidance and support. I appreciate your patience and input when I get lost, the discussions about my research and being a scientist.

Thanks also to:

My co-supervisor Anders Lorén, it was fun doing the GC-MS experiments together. Andreas Schaefer, for all your help in so many different matters.

My examiner Hanna Härelind, for evaluating my research progress and for leading the Division of Applied Chemistry and the Department of Chemistry and Chemical Engineering.

My director of studies Lars Evenäs, for your help and your dedication to us PhD students.

Lasse Urholm and Lennart Norberg for your help with the reactors, their equipment and fixing their many failures.

All my current and previous colleagues at KCK and TYK, the KB PhD council and the Doctoral Students' Guild for a good atmosphere including all the fikas, sport sessions, after works, games and discussions. I want to thank Alvaro, Andreas, Anna, Carl-Robert, Caroline, Cedrik, Eduardo, Elyse, Felix, Giulio, Gunnar, Johanna, Jojo, Lars, Leo, Lynga, Mats, Milene, Noemi, Peter, Rebekah, Saba, Simone, Xuětíng and Yanyue.

My very special thanks to Felix and Xuětíng for your helping hands and minds in endless lab sessions and discussions about my research problems.

I am grateful for my friends in and outside of Chalmers, for your love and for letting me have a good time with you during and after my studies.

Finally, I want to thank my family for your love and everything you have provided me with throughout my life.

Christopher Sauer, Göteborg, March 2021

Bibliography

[1] Hannah Ritchie Max Roser and Esteban Ortiz-Ospina. 'World Population Growth'. In: *Our World in Data* (2013). https://ourworldindata.org/world-population-growth (cit. on p. 1).

[2] K. Haustein et al. 'A real-time Global Warming Index'. In: *Scientific Reports* 7.1 (Dec. 2017), pp. 1–6. DOI: 10.1038/s41598-017-14828-5 (cit. on p. 1).

[3] Bradley J. Cardinale et al. 'Biodiversity loss and its impact on humanity'. In: *Nature* 486.7401 (June 2012), pp. 59–67. DOI: 10.1038/nature11148 (cit. on p. 1).

[4] *A European Green Deal | European Commission*. URL: https://ec.europa.eu/info/strategy/priorities-2019-2024/european-green-deal_en (cit. on p. 1).

[5] *Urban Dictionary: catalyst*. URL: https://www.urbandictionary.com/define.php?term=catalyst&utm_source=search-action (cit. on p. 1).

[6] I. Chorkendorff and J. W. Niemantsverdriet. 'Oil Refining and Petrochemistry'. In: *Concepts of Modern Catalysis and Kinetics*. John Wiley & Sons, Ltd, 2005. Chap. 9, pp. 349–376. DOI: 10.1002/3527602658.ch9 (cit. on p. 1).

[7] V. Smil. 'Detonator of the population explosion'. In: *Nature* 400.6743 (July 1999), p. 415. DOI: 10.1038/22672 (cit. on p. 1).

[8] Hideshi Hattori. 'Solid acid catalysts: Roles in chemical industries and new concepts'. In: *Topics in Catalysis*. Vol. 53. 7-10. Kluwer Academic Publishers, June 2010, pp. 432–438. DOI: 10.1007/s11244-010-9469-9 (cit. on pp. 2, 4).

[9] 'Global climate strike'. In: *Nature Catalysis* 2.10 (Oct. 2019), p. 831. DOI: 10.1038/s41929-019-0374-8 (cit. on p. 2).

[10] George W. Huber, Sara Iborra and Avelino Corma. 'Synthesis of transportation fuels from biomass: Chemistry, catalysts, and engineering'. In: *Chemical Reviews* 106.9 (Sept. 2006), pp. 4044–4098. DOI: 10.1021/cr068360d (cit. on p. 3).

[11] Joseph J. Bozell and Gene R. Petersen. 'Technology development for the production of biobased products from biorefinery carbohydrates - The US Department of Energy's "top 10" revisited'. In: *Green Chemistry* 12.4 (2010), pp. 539–554. DOI: 10.1039/b922014c (cit. on p. 3).

[12] Michèle Besson, Pierre Gallezot and Catherine Pinel. 'Conversion of Biomass into Chemicals over Metal Catalysts'. In: *Chemical Reviews* 114.3 (2014). PMID: 24083630, pp. 1827–1870. DOI: 10.1021/cr4002269 (cit. on p. 3).

[13] Manuel Moliner, Yuriy Román-Leshkov and Mark E. Davis. 'Tin-containing zeolites are highly active catalysts for the isomerization of glucose in water'. In: *Proceedings of the National Academy of Sciences* 107.14 (Apr. 2010), pp. 6164–6168. DOI: 10.1073/PNAS.1002358107 (cit. on p. 3).

[14] Yuriy Román-Leshkov, Juben N Chheda and James A Dumesic. 'Phase Modifiers Promote Efficient Production of Hydroxymethylfurfural from Fructose'. In: *Science* 312.5782 (June 2006), p. 1933. DOI: 10.1126/science.1126337 (cit. on p. 3).

[15] Guang-Hui Wang et al. 'Platinum–cobalt bimetallic nanoparticles in hollow carbon nanospheres for hydrogenolysis of 5-hydroxymethylfurfural'. In: *Nature Materials* 13.3 (2014), pp. 293–300. DOI: 10.1038/nmat3872 (cit. on p. 3).

[16] George W. Huber, Sara Iborra and Avelino Corma. 'Synthesis of Transportation Fuels from Biomass: Chemistry, Catalysts, and Engineering'. In: *Chemical Reviews* 106.9 (2006). PMID: 16967928, pp. 4044–4098. DOI: 10.1021/cr068360d (cit. on p. 3).

[17] Axel Fredric Cronstedt. *Rön och beskrifning om en obekant bärg art, som kallas Zeolites*. Vol. 17. Svenska Vetenskaps Akademiens Handlingar Stockholm, 1756 (cit. on p. 3).

[18] Ch. Baerlocher and L.B. McCusker. *Database of Zeolite Structures*. URL: http://www.iza-structure.org/databases/ (cit. on p. 4).

[19] Hideshi Hattori and Yoshio Ono. 'Catalysts and catalysis for acid-base reactions'. In: *Metal Oxides in Heterogeneous Catalysis*. Elsevier, Jan. 2018, pp. 133–209. DOI: 10.1016/B978-0-12-811631-9.00004-1 (cit. on pp. 4, 25).

[20] Jiři Čejka, Avelino Corma and Stacey Zones. *Zeolites and Catalysis*. Ed. by Jiři Čejka, Avelino Corma and Stacey Zones. Vol. 1-2. Wiley, Apr. 2010 (cit. on pp. 4, 25).

[21] Jiří Čejka, Russell E Morris and Petr Nachtigall, eds. *Zeolites in Catalysis. Properties and Applications*. Catalysis Series. The Royal Society of Chemistry, 2017, P001–527 (cit. on p. 4).

[22] N. V. Choudary and B. L. Newalkar. 'Use of zeolites in petroleum refining and petrochemical processes: Recent advances'. In: *Journal of Porous Materials* 18.6 (Dec. 2011), pp. 685–692. DOI: 10.1007/s10934-010-9427-8 (cit. on p. 4).

[23] S. Matar and L.F. Hatch. *Chemistry of petrochemical processes*. Chemical, Petrochemical & Process. Gulf Professional Pub., 2001 (cit. on p. 5).

[24] The Business Research Company. 2018. URL: https://www.thebusinessresearchcompany.com/report/aromatics-global-market-briefing-2018 (visited on 04/04/2020) (cit. on p. 5).

[25] Alexander M. Niziolek et al. 'Biomass-Based Production of Benzene, Toluene, and Xylenes via Methanol: Process Synthesis and Deterministic Global Optimization'. In: *Energy and Fuels* 30.6 (June 2016), pp. 4970–4998. DOI: 10.1021/acs.energyfuels.6b00619 (cit. on p. 5).

[26] Aromatics Producers Association (APA) - CEFIC. 2001. URL: https://www.petrochemistry.eu/wp-content/uploads/2018/01/APAEN.pdf (visited on 04/04/2020) (cit. on p. 5).

[27] W. A. Sweeney and P. F. Bryan. 'BTX Processing'. In: *Kirk-Othmer Encyclopedia of Chemical Technology*. American Cancer Society, 2000. DOI: 10.1002/0471238961.02202419230505.a01 (cit. on p. 5).

[28] Amy E. Settle et al. 'Heterogeneous Diels-Alder catalysis for biomass-derived aromatic compounds'. In: *Green Chemistry* 19.15 (2017), pp. 3468–3492. DOI: 10.1039/c7gc00992e (cit. on p. 5).

[29] Nima Nikbin et al. 'A DFT study of the acid-catalyzed conversion of 2,5-dimethylfuran and ethylene to p-xylene'. In: *Journal of Catalysis* 297 (Jan. 2013), pp. 35–43. DOI: 10.1016/j.jcat.2012.09.017 (cit. on p. 5).

[30] Ryan E. Patet et al. 'Kinetic Regime Change in the Tandem Dehydrative Aromatization of Furan Diels–Alder Products'. In: *ACS Catalysis* 5.4 (Apr. 2015), pp. 2367–2375. DOI: 10.1021/cs5020783 (cit. on pp. 5, 6, 18).

[31] C. Luke Williams et al. 'Kinetic regimes in the tandem reactions of H-BEA catalyzed formation of p-xylene from dimethylfuran'. In: *Catalysis Science and Technology* 6.1 (Jan. 2016), pp. 178–187. DOI: 10.1039/c5cy01320h (cit. on p. 5).

[32] Saikat Dutta and Navya Subray Bhat. 'Catalytic synthesis of renewable p-xylene from biomass-derived 2,5-dimethylfuran: a mini review'. In: *Biomass Conversion and Biorefinery* (2020). DOI: 10.1007/s13399-020-01042-z (cit. on p. 5).

[33] Chun-Chih Chang et al. 'Ultra-selective cycloaddition of dimethylfuran for renewable p-xylene with H-BEA'. In: *Green Chem.* 16.2 (Jan. 2014), pp. 585–588. DOI: 10.1039/C3GC40740C (cit. on pp. 5, 6, 12, 26).

[34] Xinqiang Feng et al. 'Ultra-selective p-xylene production through cycloaddition and dehydration of 2,5-dimethylfuran and ethylene over tin phosphate'. In: *Applied Catalysis B: Environmental* 259 (Dec. 2019), p. 118108. DOI: 10.1016/j.apcatb.2019.118108 (cit. on p. 5).

[35] George W. W. Huber and Avelino Corma. 'Synergies between bio- and oil refineries for the production of fuels from biomass'. In: *Angewandte Chemie - International Edition* 46.38 (Sept. 2007), pp. 7184–7201. DOI: 10.1002/anie.200604504 (cit. on p. 6).

[36] Torren R. R. Carlson, Tushar P. P. Vispute and George W. W. Huber. 'Green gasoline by catalytic fast pyrolysis of solid biomass derived compounds.' In: *ChemSusChem* 1.5 (May 2008), pp. 397–400. DOI: 10.1002/cssc.200800018 (cit. on p. 6).

[37] Yu Ting Cheng and George W. Huber. 'Chemistry of furan conversion into aromatics and olefins over HZSM-5: A model biomass conversion reaction'. In: *ACS Catalysis* 1.6 (June 2011), pp. 611–628. DOI: 10.1021/cs200103j (cit. on pp. 6, 17, 23, 25).

[38] Evgeny A. Uslamin et al. 'Catalytic conversion of furanic compounds over Ga-modified ZSM-5 zeolites as a route to biomass-derived aromatics'. In: *Green Chemistry* 20.16 (2018), pp. 3818–3827. DOI: 10.1039/C8GC01528G (cit. on pp. 6, 17, 24–26, 28).

[39] Evgeny A. Uslamin et al. 'Gallium-promoted HZSM-5 zeolites as efficient catalysts for the aromatization of biomass-derived furans'. In: *Chemical Engineering Science* 198 (Apr. 2019), pp. 305–316. DOI: 10.1016/j.ces.2018.09.023 (cit. on pp. 6, 25).

[40] Inc Anellotech. *Chemicals | Anellotech, Inc | Cost Competitive Bio-Sourced Chemicals and Fuels*. URL: https://www.anellotech.com/ (cit. on p. 6).

[41] *Virent, Inc.* URL: https://www.virent.com/ (cit. on p. 6).

[42] Yu Ting Cheng and George W. Huber. 'Production of targeted aromatics by using Diels-Alder classes of reactions with furans and olefins over ZSM-5'. In: *Green Chemistry* 14.11 (Oct. 2012), pp. 3114–3125. DOI: 10.1039/c2gc35767d (cit. on pp. 6, 12, 17, 24–26).

[43] Yu-Ting Cheng et al. 'Production of Renewable Aromatic Compounds by Catalytic Fast Pyrolysis of Lignocellulosic Biomass with Bifunctional Ga/ZSM-5 Catalysts'. In: *Angewandte Chemie* 124.6 (Feb. 2012), pp. 1416–1419. DOI: 10.1002/ange.201107390 (cit. on pp. 6, 25).

[44] Jinsheng Gou et al. 'The effects of ZSM-5 mesoporosity and morphology on the catalytic fast pyrolysis of furan'. In: *Green Chemistry* 19.15 (July 2017), pp. 3549–3557. DOI: 10.1039/C7GC01395G (cit. on p. 6).

[45] Lijuan Zhu et al. 'Selective conversion of furans to p-xylene with surface-modified zeolites'. In: *Journal of Chemical Technology and Biotechnology* 94.9 (Sept. 2019), pp. 2876–2887. DOI: 10.1002/jctb.6090 (cit. on p. 6).

[46] Evgeny A. Uslamin et al. 'Co-Aromatization of Furan and Methanol over ZSM-5—A Pathway to Bio-Aromatics'. In: *ACS Catalysis* 9.9 (Sept. 2019), pp. 8547–8554. DOI: 10.1021/acscatal.9b02259 (cit. on p. 6).

[47] Evgeny A Uslamin et al. 'Aromatization of ethylene over zeolite-based catalysts'. In: *Catalysis Science & Technology* 10.9 (2020), pp. 2774–2785. DOI: 10.1039/C9CY02108F (cit. on p. 6).

[48] Thomas G. Mayerhöfer, Susanne Pahlow and Jürgen Popp. 'The Bouguer-Beer-Lambert Law: Shining Light on the Obscure'. In: *ChemPhysChem* 21.18 (Sept. 2020), pp. 2029–2046. DOI: 10.1002/cphc.202000464 (cit. on p. 9).

[49] Peter J. Larkin. 'General Outline for IR and Raman Spectral Interpretation'. In: *Infrared and Raman Spectroscopy*. Elsevier, Jan. 2018, pp. 135–151. DOI: 10.1016/b978-0-12-804162-8.00007-0 (cit. on p. 10).

[50] D. Bassi, P. Tosi and R. Schlögl. 'Ion-molecule-reaction mass spectrometer for on-line gas analysis'. In: *Journal of Vacuum Science & Technology A: Vacuum, Surfaces, and Films* 16.1 (Jan. 1998), pp. 114–122. DOI: 10.1116/1.580957 (cit. on pp. 11, 12).

[51] Cyrill Hornuss et al. 'Real-time monitoring of propofol in expired air in humans undergoing total intravenous anesthesia'. In: *Anesthesiology* 106.4 (Apr. 2007), pp. 665–674. DOI: 10.1097/01.anes.0000264746.01393.e0 (cit. on p. 12).

[52] Xueting Wang et al. 'Methanol Desorption from Cu-ZSM-5 Studied by in Situ Infrared Spectroscopy and First-Principles Calculations'. In: *Journal of Physical Chemistry C* 121.49 (Dec. 2017), pp. 27389–27398. DOI: 10.1021/acs.jpcc.7b07067 (cit. on pp. 12, 28).

[53] Carl L. Yaws. Knovel, 2014. (Visited on 02/04/2020) (cit. on p. 13).

[54] Qiang Lu et al. 'Catalytic Fast Pyrolysis of Biomass Impregnated with Potassium Phosphate in a Hydrogen Atmosphere for the Production of Phenol and Activated Carbon'. In: *Frontiers in Chemistry* 6 (Feb. 2018), p. 32. DOI: 10.3389/fchem.2018.00032 (cit. on p. 17).

[55] Juliana S Espindola et al. 'Conversion of furan over gallium and zinc promoted ZSM-5: The effect of metal and acid sites'. In: *Fuel Processing Technology* 201.August 2019 (2020), p. 106319. DOI: 10.1016/j.fuproc.2019.106319 (cit. on pp. 17, 24–26).

[56] Hongkui. Xiao, Steven P Levine and James B D'Arcy. 'Iterative least-squares fit procedures for the identification of organic vapor mixtures by Fourier-transform infrared spectrophotometry'. In: *Analytical Chemistry* 61.24 (1989), pp. 2708–2714. DOI: 10.1021/ac00199a006 (cit. on p. 21).

[57] Christopher J. Gilbert et al. 'The effect of water on furan conversion over ZSM-5'. In: *ChemCatChem* 6.9 (Sept. 2014), pp. 2497–2500. DOI: 10.1002/cctc.201402390 (cit. on p. 25).

[58] Haojie Fan et al. 'Catalytic pyrolysis of agricultural and forestry wastes in a fixed-bed reactor using K2CO3 as the catalyst'. In: *Waste Management and Research* 38.1 (2020), pp. 78–87. DOI: 10.1177/0734242X19875508 (cit. on pp. 25, 26).

[59] Baptiste Sirjean and René Fournet. 'Unimolecular decomposition of 2,5-dimethylfuran: A theoretical chemical kinetic study'. In: *Physical Chemistry Chemical Physics* 15.2 (Jan. 2013), pp. 596–611. DOI: 10.1039/c2cp41927k (cit. on p. 25).

[60] Jiabin Yin et al. 'Highly Selective Production of p-Xylene from 2,5-Dimethylfuran over Hierarchical NbOx-Based Catalyst'. In: *ACS Sustainable Chemistry and Engineering* 6.2 (Feb. 2018), pp. 1891–1899. DOI: 10.1021/acssuschemeng.7b03297 (cit. on p. 26).

[61] Dong Wang et al. 'Selective production of aromatics from alkylfurans over solid acid catalysts'. In: *ChemCatChem* 5.7 (July 2013), pp. 2044–2050. DOI: 10.1002/cctc.201200757 (cit. on p. 26).

[62] Wenliang Wang et al. 'Catalytic fast pyrolysis of cellulose for increasing contents of furans and aromatics in biofuel production'. In: *Journal of Analytical and Applied Pyrolysis* 131 (May 2018), pp. 93–100. DOI: 10.1016/j.jaap.2018.02.004 (cit. on p. 26).

[63] Qiang Lu et al. 'Catalytic Upgrading of Biomass Fast Pyrolysis Vapors with Nano Metal Oxides: An Analytical Py-GC/MS Study'. In: 3 (2010), pp. 1805–1820. DOI: 10.3390/en3111805 (cit. on p. 26).

[64] Joel McGlone et al. 'Desilicated ZSM-5 Zeolites for the Production of Renewable p-Xylene via Diels–Alder Cycloaddition of Dimethylfuran and Ethylene'. In: *Catalysts* 8.6 (June 2018), p. 253. DOI: 10.3390/catal8060253 (cit. on p. 26).

[65] Chun-Chih Chang et al. 'Lewis acid zeolites for tandem Diels–Alder cycloaddition and dehydration of biomass-derived dimethylfuran and ethylene to renewable p-xylene'. In: *Green Chemistry* 18.5 (Feb. 2016), pp. 1368–1376. DOI: 10.1039/C5GC02164B (cit. on p. 26).

[66] Ludmila Kubelková, Jiří Čejka and Jana Nováková. 'Surface reactivity of ZSM-5 zeolites in interaction with ketones at ambient temperature (a FT-i.r. study)'. In: *Zeolites* 11.1 (Jan. 1991), pp. 48–53. DOI: 10.1016/0144-2449(91)80355-4 (cit. on p. 27).

[67] Mark A. Newton et al. 'Active sites and mechanisms in the direct conversion of methane to methanol using Cu in zeolitic hosts: A critical examination'. In: *Chemical Society Reviews* 49.5 (Mar. 2020), pp. 1449–1486. DOI: 10.1039/c7cs00709d (cit. on p. 28).

[68] Jana Engeldinger et al. 'Elucidating the role of Cu species in the oxidative carbonylation of methanol to dimethyl carbonate on CuY: An in situ spectroscopic and catalytic study'. In: *Applied Catalysis A: General* 382.2 (July 2010), pp. 303–311. DOI: 10.1016/j.apcata.2010.05.009 (cit. on p. 28).

[69] I Kiricsi et al. 'Progress toward Understanding Zeolite .beta. Acidity: An IR and 27Al NMR Spectroscopic Study'. In: *The Journal of Physical Chemistry* 98.17 (Apr. 1994), pp. 4627–4634. DOI: 10.1021/j100068a024 (cit. on p. 29).

[70] Dominique M Roberge, Heike Hausmann and Wolfgang F Hölderich. 'Dealumination of zeolite beta by acid leaching: a new insight with two-dimensional multi-quantum and cross polarization 27Al MAS NMR'. In: *Phys. Chem. Chem. Phys.* 4.13 (2002), pp. 3128–3135. DOI: 10.1039/B110679C (cit. on p. 29).

[71] Anton A. Gabrienko et al. 'Strong acidity of silanol groups of zeolite beta: Evidence from the studies by IR spectroscopy of adsorbed CO and 1H MAS NMR'. In: *Microporous and Mesoporous Materials* 131.1-3 (June 2010), pp. 210–216. DOI: 10.1016/j.micromeso.2009.12.025 (cit. on p. 29).